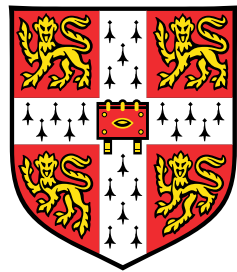


Modelling lung health in Cystic Fibrosis using machine learning analysis of home monitoring data



Tristan Trébaol

Department of Medicine
University of Cambridge

This dissertation is submitted for the degree of

Doctor of Philosophy

Queen's College

April 2025

I would like to dedicate this thesis to my loving parents ...

Declaration

I hereby declare that except where specific reference is made to the work of others, the contents of this dissertation are original and have not been submitted in whole or in part for consideration for any other degree or qualification in this, or any other university. This dissertation is my own work and contains nothing which is the outcome of work done in collaboration with others, except as specified in the text and Acknowledgements. This dissertation contains fewer than 65,000 words including appendices, bibliography, footnotes, tables and equations and has fewer than 150 figures.

Tristan Trébaol
April 2025

Acknowledgements

And I would like to acknowledge ...

Abstract

This is where you write your abstract ...

Table of contents

| | |
|---|-------------|
| List of figures | xiii |
| List of tables | xvii |
| Nomenclature | xix |
| 1 Modelling lung health at one point in time | 1 |
| 1.1 Model structure definition | 1 |
| 1.1.1 Dealing with complex systems modellisation | 1 |
| 1.1.2 Time constraint: studying lung health at one point in time | 2 |
| 1.1.3 Space constraint: selecting two observables | 2 |
| 1.1.4 Analysing the relationship between FEV ₁ , oxygen saturation, and lung health | 4 |
| 1.2 Modelling the health of the conducting zone with FEV ₁ | 6 |
| 1.2.1 Determining the structure of the graph from physiology knowledge | 6 |
| 1.2.2 Data validation of the multiplicative factor | 8 |
| 1.3 Conditional probability tables | 13 |
| 1.3.1 Modelling an individual's healthy FEV ₁ prior | 13 |
| 1.3.2 Multiplicative factor to encode P(FEV ₁ healthy FEV ₁ , airway resistance) | 14 |
| 1.3.3 Modelling the variability in FEV ₁ | 16 |
| 1.4 Characterising the health of the respiratory zone with oxygen saturation . . | 19 |
| 1.4.1 Structuring the relationship between oxygen saturation and lung health using physiology knowledge | 19 |
| 1.4.2 Data validation of the oxygen saturation side of the model | 22 |
| 1.5 Conditional probability tables for the oxygen saturation side | 26 |
| 1.5.1 Modelling an individual's healthy oxygen saturation prior | 27 |
| 1.5.2 The drop in oxygen saturation due to airway resistance | 31 |

| | | |
|--|--|-----------|
| 1.5.3 | Oxygen saturation noise model | 35 |
| 1.5.4 | Multiplicative drop in oxygen saturation due to inactive alveoli | 39 |
| 1.6 | A web-application for interactive inference | 39 |
| 1.7 | Model validation and usefulness | 39 |
| 1.7.1 | Structural validation | 40 |
| 1.7.2 | Domain expert inference evaluation and early diagnostic model capacity | 40 |
| 1.7.3 | Validation against synthetically generated data | 42 |
| 1.8 | Opportunities of model applications in healthcare | 45 |
| 1.8.1 | An digital app to let patient take ownership of their health | 45 |
| 1.8.2 | A digital app to democratise access to healthcare | 46 |
| 1.8.3 | Population assessment and clinical-trial monitoring | 46 |
| 1.8.4 | Clinical trial monitoring | 48 |
| 1.9 | Model limitations | 48 |
| 1.9.1 | Incapacity to identify small healthy lungs from big lungs with disease | 48 |
| 1.9.2 | Incapacity to fully differentiate SpO ₂ drop due to airway resistance or inactive alveoli | 49 |
| 1.9.3 | Lack of ground truth validation for inferred lung metrics | 49 |
| 1.9.4 | Difficulties in modelling non-linear phenomena | 50 |
| 1.10 | Conclusion | 50 |
| References | | 53 |
| Appendix A Multiplying two uniformly distributed random variables | | 55 |

List of figures

| | | |
|-----|---|----|
| 1.1 | Scatter plot of O ₂ saturation and FEV ₁ smoothed. On both axis, the red distribution shifts to lower values. This means that O ₂ saturation and FEV ₁ values tend to drop from baseline during exacerbations. | 4 |
| 1.2 | Graphical structure of the FEV ₁ side of the model | 8 |
| 1.3 | Focus on the update of the graph from Figure 1.2 where I would differentiate the airway resistance into its reversible component (small airway blockage) and permanent component (long term lung damage). The rest of the graph would remain the same | 9 |
| 1.4 | Relationship between permanent lung damage approximated from the data and age. One can observe a clear increase of lung damage with the mean group's age from 44% in age group [18-30), to 49% in age group [30-40) and 55% in age group [40-50) | 11 |
| 1.5 | Relationship between the small airway blockage approximated from the data and the exacerbation labels from the predictive classifier in [?]. One bar is one individual, the results are presented in Table 1.1 | 12 |
| 1.6 | Analytical solution (red) against sampling solution (blue) to the multiplication of two uniformly distributed random variables. Example for healthy FEV ₁ in the range 4.40-4.45 L and airway resistance in the range 44-46%. With $FEV_1 = HFEV_1(1-AR)$, the resulting FEV ₁ is indeed defined from 2.288 to 2.403 L | 15 |
| 1.7 | Variability model to encode $P(ecFEV_1 uFEV_1)$. A shows that the individual-level std of the ecFEV ₁ residuals' increases with ecFEV ₁ . This justifies using a gaussian model with an additive and a multiplicative component: $\mathcal{N}(uFEV_1, a uFEV_1 + b)$. B shows the result of the regression going through the mid-bin of each group, hereby setting the gaussian noise parameters to a=0.00510174 and b=0.03032977 | 18 |

| | | |
|------|--|----|
| 1.8 | Model structure with the FEV ₁ and the oxygen saturation side (extension from 1.2 | 21 |
| 1.9 | Visualisation of the predicted oxygen saturation during exacerbated and stable period for every individual, ordered by an overall measure of CF small airway disease severity. I added the mean, highlighted by the dotted line, on the boxplots. The green horizontal line shows the limit for normal SpO ₂ adjusted to after the correction by the sex bias. | 23 |
| 1.10 | Visualisation of the predicted oxygen saturation during exacerbated and stable period for every individual, ordered by an overall measure of CF small airway disease severity. I added the mean, highlighted by the dotted line, on the boxplots. The green horizontal line shows the limit for normal SpO ₂ adjusted to after the correction by the sex bias. | 25 |
| 1.11 | Healthy O ₂ saturation fit according to equations 1.11: evolution of the regression parameters with increasing individuals' healthiness threshold. The coloured rectangle represents range of values seen in healthy populations (CITE). The blue and red curves increase monotonically and, doing so, converge to values from literature after the 80% healthiness threshold. This indicates that the healthier the individuals, the higher the O ₂ saturation. . . | 30 |
| 1.12 | Relationship between O ₂ Sat% and airway resistance. Values in 100-102% appear when O ₂ saturation measurements are larger than their healthy values. This happens when the measured O ₂ saturation is above its true value (due to measurement noise) or when the HO2Sat value (taken as the distribution's mean) is below its true value, or a combination of both effects. The curve traced by the highest points, excluding the first 1-5 outliers, is roughly constant up to 40% airway resistance then it slowly decreases, with few data above 70%. Points are displayed with 30% opacity, which allows to differentiate one, two, and three or more superimposing points. | 32 |
| 1.13 | Evolution of the maximum achievable O ₂ Sat% with airway resistance, and associated data scarcity. The fitted black curve (A) is constant up to 35% airway resistance, then slowly decreases until 70%. Past 70% of airway resistance too few data-points (B) with too few contributing individuals (C) were collected to draw a reliable curve. | 34 |

| | |
|--|----|
| 1.14 Factor function F4: evolution of the multiplicative drop from healthy O ₂ saturation with airway resistance. Three zones can be observed: 1) 0%-35% where airway resistance has no impact on healthy O ₂ saturation, 2) 35%-70% where airway resistance reduces healthy O ₂ saturation, and 3) above 70% where the fit is unreliable because of too few data-points. | 35 |
| 1.15 Histogram of the standard deviation of O ₂ saturation measurements for each Breathe's individual. The average standard deviation in this sub-population is 0.9. 54/213 individuals were included after applying the healthiness and the data density filters. | 38 |
| 1.16 Results of inference using the O ₂ saturation noise model. The variables' discretisation parameters are set according to table ??.. | 38 |
| 1.17 Synthetic data vs real data comparison. – I address the middle plot later on in the section | 43 |
| 1.18 Population-level density profile of airway resistance and inactive alveoli in Breathe vs smartcare | 47 |

List of tables

| | | |
|-----|--|----|
| 1.1 | Results of grouping individuals in Figure 1.5 with similar behaviours. The majority of the individuals have a higher small airway blockage during exacerbations. It confirms that exacerbations tend to correlate with small airway blockage. | 12 |
| 1.2 | Bootstrapped Pearson correlation coefficients between healthy O ₂ saturation and lung size for 213 individuals. Healthy O ₂ saturation is estimated by a robust maximum for O ₂ saturation, defined as the individual's 5 th highest measured value. Lung size is approximated by height and predicted FEV ₁ and appears strongly and negatively correlated with O ₂ saturation. After correction by sex, a strong evidence of weak correlation remains for height, but not for predicted FEV ₁ as the range crosses 0. | 29 |

Nomenclature

Acronyms / Abbreviations

ABG Arterial Blood Gas

DLCO Diffusing Capacity of the Lung for Carbon Monoxide

GLI Global Lung Initiative

Chapter 1

Modelling lung health at one point in time

1.1 Model structure definition

1.1.1 Dealing with complex systems modellisation

There are three main layers of complexity in this project.

Firstly, the lungs are incredibly complex organs. I have made an exhaustive description, in Section X, of the many mechanistic models of the lungs that were developed, involving advanced fluid mechanics and partial differential equations. Although these models grew in complexity over the years, as researchers were building on top of the previous work, the state of the art still misses relatively important biological mechanisms (cite X).

The second layer of complexity is related to the particularities of dealing with the challenges of medical datasets. I have access to two rich data-sets from CF home-monitoring studies, described in Section X. There has been extensive dedication to validate and process these data (mostly as part of one thesis - cite X). However, asking a different research question means uncovering unexplored subsets of the data, which brings back considerable effort for data wrangling, sanitisation, and pipelining.

The third layer of complexity arises from the dual constraint imposed by integrating physiological theory and empirical data.

an in-depth understanding of respiratory physiology with advanced data-science methodologies

making the medical model and the data model converge.

I cannot encode a mechanism expected by pulmonary physiology if the corresponding signal is absent from the data. Conversely, I cannot model a statistical pattern for which no pathophysiological explanation exists. This bidirectional requirement allows to build an highly interpretable foundational model that is sensitive to genuine physiological signal.

Achieving this integration necessitates extensive theoretical and clinical expertise in pulmonary medicine, as well as a robust foundation in machine learning, computational modeling, and quantitative analysis.

Because the available measurements are sparse, noisy, and only indirectly related to the underlying processes, I must augment them with detailed knowledge of pulmonary physiology to extract reliable and clinically meaningful insights into lung health.

The third layer of complexity, which is also the main challenge of this project, resides in integrating an in-depth understanding of respiratory physiology with advanced data-science methodologies. Achieving this integration necessitates extensive theoretical and clinical expertise in pulmonary medicine, as well as a robust foundation in machine learning, computational modeling, and quantitative analysis. The convergence of these two domains underscores the core complexity of the work.

Selecting an appropriate level of model complexity is thus pivotal to the success of this research. This is especially true when, to my knowledge, this work represents the first attempt to leverage pulmonary physiology for interpreting noisy, incomplete longitudinal lung-health data. Consequently, a primary concern was determining whether such a model could be both feasible and clinically useful.

I believe that a complex model that works always originates from a simple model that worked. Hence, I began by specifying minimal requirements necessary for meaningful healthcare applications. For this initial chapter, I therefore imposed constraints on both the temporal and spatial dimensions of the model.

1.1.2 Time constraint: studying lung health at one point in time

A simple and meaningful time constraint is to start by building a model that can only read one set of measurements; as a doctor that would meet a person for the first time, without access to their medical history, and would aim to understand their lung health running only a few tests.

1.1.3 Space constraint: selecting two observables

The space constraint relates to the number of tests that the doctor can run to collect their evidence. The few selected health metrics should be the ones that can explain most variability in lung health. In section X, I presented the Weibel model of the respiratory airway tree which is well-known in respiratory physiology. It divides the lungs into two main zones: the conductive zone where the transport of oxygen is driven by airflow and the respiratory

zone where the transport of oxygen is driven by diffusion. Intuitively, I assumed that one physiological measure would explain at most one underlying physical mechanism of lung health. At least two measures would therefore be needed to find a complete picture of lung health, one for each broad region of the airway tree.

Describing the health of the conducting zone The choice of the measure to describe the health of the conducting zone is straightforward. FEV₁ is the "gold standard" in CF health monitoring and other obstructive lung diseases such as COPD (section X). Precisely, FEV₁ is a measure of how resistive the airways are during a forced expiration. The Hagen-Poiseuille equation introduced in section X links the resistance with the delta of pressure that drives airflow. Additionally, FEV₁ is relatively easy to measure with a spirometer, a small device that is inexpensive compared to hospital equipments.

Describing the health of the respiratory zone For the respiratory zone, selecting an appropriate test proves more challenging. In an ideal scenario, a physician would administer a DLCO (Diffusing Capacity of the Lung for Carbon Monoxide) test. This test necessitates specialized pulmonary function equipment such as spirometers, gas analyzers with calibrated mixtures, and dedicated software (cite X), and thus cannot be performed inexpensively at home as required by the project's aim. Since oxygen diffuses into the bloodstream at the alveolar level, blood oxygenation offers the next most direct insight into respiratory-zone function. However, monitoring blood oxygenation is not sufficient on its own to assess the health of the respiratory zone because it involves the whole process of oxygen transport. An abnormal result could stem from obstructions in the upper airways (e.g., during a severe asthma episode) even if alveolar gas exchange is normal.

To assess blood oxygenation directly, the gold-standard approach would be an Arterial Blood Gas (ABG) test, which measures the partial pressure of oxygen (PaO₂) and the arterial oxygen saturation (cite X). Yet ABG also requires costly equipment, blood samples, and specialised staff. Consequently, the most practical alternative is to measure peripheral capillary oxygen saturation (SpO₂), also termed oxygen saturation, a widely used, non-invasive test. Physicians routinely measure it in various clinical settings (e.g., during initial consultations or while monitoring a hospitalised patient's vital signs). Moreover, certain smartwatches now estimate SpO₂ (cite X), although typically with less accuracy than medical-grade pulse oximeters (cite X).

Although one can theoretically back-calculate PaO₂ from SpO₂ via the oxyhemoglobin-dissociation curve (section X), discuss explain in section X the reasons for not doing so. To conclude, from the standpoint of pulmonary physiology and clinical feasibility, the simplest

yet meaningful approach to capturing lung health at a single time point involves measuring FEV₁ (for the conducting zone) and oxygen saturation (for the respiratory zone).

1.1.4 Analysing the relationship between FEV₁, oxygen saturation, and lung health

The conclusion of the previous section essentially assumes that FEV₁ and oxygen saturation are key physiological indicators of lung function. I now have to confirm this assumption drawn from pulmonary physiology knowledge by analysing real patient data. I therefore plotted FEV₁ versus oxygen saturation for individuals with varying severities of lung disease. I have chosen the data from the SmartCare study, over BreatheCF, because i) it contains sicker individuals with interesting examples of very unhealthy lungs, ii) every day has an extra label *Is Exacerbated* which tells whether or not the individual was having an acute pulmonary exacerbation. This label was learnt by the acute pulmonary exacerbation prediction model introduced in section X. The result on Figure 1.1 shows that these two metrics effectively differentiate patients based on their respiratory health.

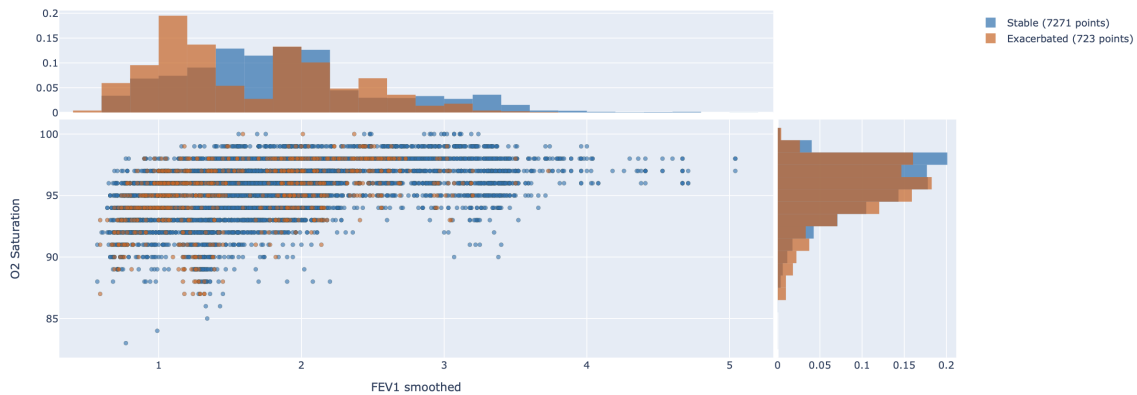


Fig. 1.1 Scatter plot of O₂ saturation and FEV₁ smoothed. On both axis, the red distribution shifts to lower values. This means that O₂ saturation and FEV₁ values tend to drop from baseline during exacerbations.

There is abundant amount of information to take away from Figure 1.1, which also shows how precious Damian's predictive algorithm is to give additional insight about the health state of the lungs.

Figure adjustments I would like to start by giving a few comments on the characteristics of the visualisation itself. The scatter plot is essentially a series of horizontal lines due to SpO₂ and FEV₁ having different resolutions. Oxygen saturation is rounded to the integer,

and FEV_1 is measured with two decimal places. Additionally, the presence of multiple overlapping data points makes it difficult to compare the data-density across the plot. To mitigate this, I lowered the markers' opacity until single isolated points remained sufficiently visible. However, I found this adjustment alone inadequate and thus incorporated density plots along both axes to more clearly represent the underlying data distribution. The density plots show that the vast majority of the datapoints are located in a region of normal oxygen saturation (above 95%), and between 1 and 2.5L of FEV_1 . Lastly, only few records were performed during a stable period (roughly 10%). To palliate the lack of red presence due to the data imbalance, I plotted the records in exacerbation period (red) on top of the records in stable period (blue). This data imbalance is also the reason why the blue density plot for FEV_1 is smoother than the red one. The red distribution has a hole between 1.4-1.8L, which I assume is more due to a lack of data recorded within this range during exacerbations rather than the manifestation of a true underlying discontinuity in FEV_1 .

Figure analysis When comparing the overlaid density plots of FEV_1 and oxygen saturation between stable and exacerbation states, measurements performed during exacerbations are generally lower than those recorded during stable periods. This is particularly striking for the y-axis where the density of the oxygen saturation decreases exponentially pasts 95%. This finding is consistent with clinical expectations: lung function and oxygenation decline during exacerbation episodes.

The high FEV_1 ($> 3.2\text{L}$), high oxygen saturation quadrant is dominated by individuals in a permanent stable state: there are mostly blue datapoints. Individuals in this region could be largely asymptomatic, with no obvious clinical symptoms such as cough, airway clearance is not productive, etc. This does not necessarily mean that their lungs are completely healthy. Subclinical lung degradation such as early bronchiectasis, inflammation, or mucus accumulation can be present even when symptoms are minimal or absent (section X).

Starting from the top right region and moving left as FEV_1 reduces, the spread of oxygen saturation increases. The overall shape of the data seems to be constrained by a linear bottom envelope, suggesting that some effects in oxygen saturation are well predicted by FEV_1 . I have not identified strong reasons for the linearity of the envelope, however it is clear that the overall phenomenon is particular to CF pathology. As explained in section X, the main driver for lung degradation in CF is cumulative small airway damage, which over many years, will affect FEV_1 . FEV_1 itself being a marker of little volume of air reaching the alveoli, the progressive reduction in FEV_1 will increase the risk of oxygen desaturation, especially during exacerbations. FEV_1 and oxygen saturation are therefore correlated.

Related to the previous point, no data points are observed in the bottom right quadrant. This absence aligns with the clinical progression of CF small airway disease, where FEV₁ and oxygen saturation are intricate, making it unlikely to observe low oxygen saturation with high FEV₁ values concurrently. For generalisation purposes, it is important to note that this phenomenon is specific to CF. For example, in pneumonia, characterised by an inflammation of the alveoli, a doctor would expect to see lower values of oxygen saturation while FEV₁ would remain high.

The mid-to-low FEV₁ region is particularly challenging to analyse in this figure. I have to highlight that it represents a population-level plot, resulting in an overlap of various CF conditions. Same FEV₁ values could be obtained for individuals with large lungs and a strong infection as well as for healthy individuals with small lungs. Missclassified records can also add noise that further harms the plot clarity.

High cumulative small airway damage, that affects oxygen saturation, may also explain why oxygen saturation fails to reach the 98–100% range at very low FEV₁ levels. As seen in the top left corner of the figure, there appears to be an upper envelope that sets the maximum achievable oxygen saturation. This effect is interesting because I have not found any literature specifically describing it. These observations suggest that analysing FEV₁ and oxygen saturation together can reveal subtle trends in lung health, that I will explore in the model development. I will further investigate this phenomenon in Section X, as it could also be linked to a bias due to the low data density in this region of the plot.

In conclusion, I have hereby demonstrated that studying FEV₁ and oxygen saturation values can show distinct trends related to diverse patterns of lung damage. This comforts that these metrics are key physiological indicators of lung function. In the rest of the chapter, I will explain how I structured the point in time model to reflect the relationships in the data. I will first build an FEV₁ model of the lungs, which I will extend to produce an oxygen saturation model of the lungs. Then I will talk about model validation, usefulness for clinical applications, and limitations.

1.2 Modelling the health of the conducting zone with FEV₁

1.2.1 Determining the structure of the graph from physiology knowledge

One value of FEV₁ does not hold much clinical meaning on its own. As described in section X, the range of FEV₁ values measured in a normal healthy population varies from two to six liters. FEV₁ has therefore to be studied in comparison to a baseline. In clinics, doctors

analyse an FEV₁ in the context of the longitudinal profile of historical FEV₁ records from the same individual (ref to treatment burden in section x). Additionally, doctors also compute the FEV₁ in percent predicted where the predicted FEV₁ comes from reference equations of normal lung function (section X). Due to the time constraints (section X), the model cannot have access to the individual's medical history. The challenge is therefore to extract as much information as possible about lung health by comparing the observed FEV₁ to a healthy baseline. What I define as a healthy baseline refers to the role of predicted FEV₁ in clinical practice. A probabilistic approach however allows me to go further by using a probability distribution to represent this baseline instead of the more standard "point estimates".

The healthy FEV₁ The reference equations for normal lung function, introduced in section X, are the result of fitting a function to a dataset of FEV₁ measurements performed on a large and diverse population of healthy individuals. Height, age, and sex were selected as parameters for the fit because they are the primary demographic determinants of lung volume and lung function. The resulting function gives the predicted FEV₁ for an individual's profile, as used in clinical practice. However, height, age, and sex are not perfect determinants of FEV₁. In other words, there is some uncertainty on the real underlying healthy FEV₁ that is not captured by those demographic parameters. I will use this uncertainty to draw a probabilistic estimate of an individual's healthy baseline. This estimate is termed "prior knowledge" of the healthy baseline because it is data-agnostic (section X).

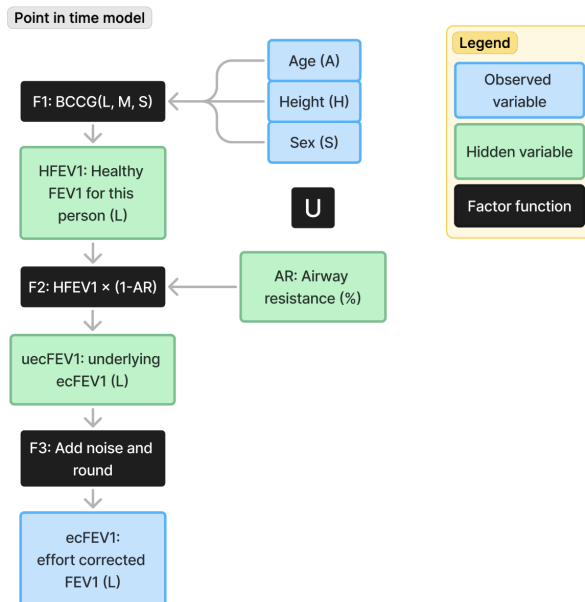
I then introduced the "healthy FEV₁" variable which represents the distribution of probable values that would be obtained by any individual (even sick) from whom one could have hypothetically reverse their lung damage. This variable will serve as the healthy baseline in the model. In theory, there is a single true underlying healthy FEV₁ for each individual. The claim from a Bayesian approach is that the more data is observed about an individual's lung and the closer the posterior of healthy FEV₁ gets to this true underlying value.

The underlying FEV₁ Defining a healthy baseline allows to address the non-pathological individual-level variability in FEV₁ (e.g. due to difference in lung size). There is also some non-pathological variability at measurement-level. It comes partly from the device technical noise, and partly from how the test is performed by the individual. I model this variability by introducing a variable connected to FEV₁, called the "underlying FEV₁", which represents the FEV₁ value that would be obtained under ideal conditions, i.e. free from any technical noise or individual variability during the forced expiratory maneuver.

Airway resistance Similarly to how doctors compute the "FEV₁ in percent predicted" by dividing the observed FEV₁ by the predicted value, I can define a "divisive measure" of the difference between healthy and underlying FEV₁ (each represented by probability distributions). Physically, FEV₁ is a measure of airway resistance, reflecting the non-linear aggregation of local resistances across the airway generation (see Section X). Consequently, this divisive measure, which expresses the drop from an individual's healthy FEV₁ baseline, can be interpreted as a probabilistic measure of the airway resistance.

I have now sufficient information to draw the first part of the model which answers the question: "What can FEV₁ tell about lung health?", see Figure 1.2.

Fig. 1.2 Graphical structure of the FEV₁ side of the model



I would like to recall that another person might have come up with another model structure. The challenge is to build a model that can be useful for clinical applications. To avoid testing numerous alternative models, I chose to develop a model based on established best practices from specialised CF centers, assuming that several decades of collaborative clinical efforts have yielded an optimal understanding of FEV₁'s role in evaluating patient health.

1.2.2 Data validation of the multiplicative factor

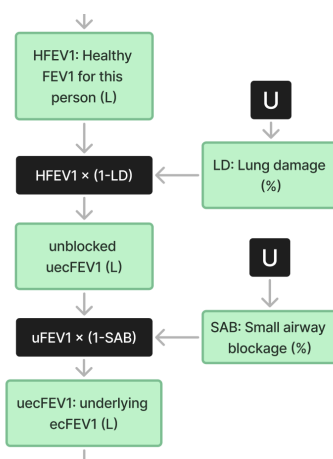
In Figure 1.2, the factors F1 and F3 are relatively straightforward to model because F1 is derived from reference equations, and F3 is essentially a noise factor. F2 is therefore the most critical to get right, as it connects the drop between healthy and observed FEV₁ with

the first health metric: airway resistance. Similarly to Section X, I produced visualisations for this factor function before implementing it to confirm that the multiplicative relationship assumption drawn from medical knowledge aligns with the actual physiological signals from the Smartcare dataset.

When developing this part of the model, I initially considered separating the airway resistance into two parts: small airway blockage and long term lung damage. This distinction is clinically significant in CF because small-airway blockage (e.g., mucus accumulation in bronchioles) can be temporary, whereas long term lung damage (e.g., bronchiectasis) is permanent. For a CF individual, it would be very informative to know what percentage of airway resistance could be reversed by changing habits (e.g., running, more physiotherapy). Likewise, monitoring the number of people at risk due to high permanent lung damage could significantly improve hospital resources management.

If the model could estimate the precise amount of reversible blockage, I could use it to introduce an additional metric called “unblocked FEV₁”. It would represent the FEV₁ a patient might achieve if all reversible components of its lung damage were resolved. Figure 1.3 shows how the airway resistance would be substituted. I decided not to do this update

Fig. 1.3 Focus on the update of the graph from Figure 1.2 where I would differentiate the airway resistance into its reversible component (small airway blockage) and permanent component (long term lung damage). The rest of the graph would remain the same



on the graph for two reasons. Firstly, the extra hidden variable would lead to too many unknowns relative to the model evidence. The updated model equations, as shown below, could not be solved by inference or would require more observables. On the left there is one

unknown for one equation, on the right there are three unknowns for two equations.

$$1 - AR = HFEV_1 \times ecFEV_1 \quad \Rightarrow \quad \begin{cases} 1 - LD = HFEV_1 \times uFEV_1 \\ 1 - SAB = uFEV_1 \times ecFEV_1 \end{cases}$$

Secondly, it is difficult to draw a clear line between permanent and reversible aspects of the airway resistance. Symptoms that should be reversible are usually never fully resolved due to the chronic aspect of the lung inflammation in CF, as explained in section X. An undetermined quantity of small airway blockage stays over long time-scales and is therefore hard to differentiate from permanent damage using the physiological signals from the dataset. I concluded that adding this complexity would not be advantageous at this stage of the project. It might however be a great candidate to extend this first model.

Nevertheless, introducing this cascade of multiplicative factors remains a compelling way to evaluate the richness of the data, that is, whether it captures different aspects of airway resistance, and to verify whether the multiplicative relationship holds in real patient data. When using data I do not have the limitations of equations and can find a reasonable approximation for the unblocked FEV₁. I did this and produced visualisations representing the multiplicative lung damage and multiplicative small-airway blockage using the SmartCare dataset. The results and interpretations for each case is described below.

Relationship between long term lung damage and age

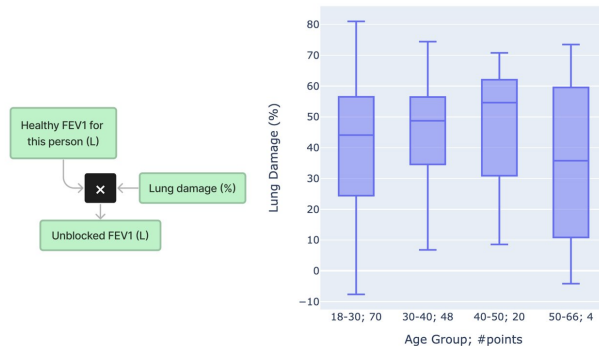
To preserve as much raw information as possible, and thus capture true signals in the data, while avoiding potentially unnecessary data processing steps, I made some approximations to identify lung damage in the data. I set an individual's healthy FEV₁ to be equal to their predicted FEV₁ as usually used in clinical practice. To estimate the unblocked FEV₁, I assumed that, over the course of the study, every individuals had performed a few FEV₁ measurements while not in an exacerbated state, i.e. without much small airway blockage. I defined the unblocked FEV₁ to be the third highest all-time FEV₁ record, thus giving one value per individual. I ignored the first and second measurements as they may be outliers. I was then able to express lung damage as a comparative measure of healthy and unblocked FEV₁. This gives:

$$(1 - \frac{uFEV_1(L)}{HFEV_1(L)}) 100 \quad (1.1)$$

Concretely, this equation means that at 0% of lung damage unblocked uFEV₁ = HFEV₁, at 25% of lung damage, uFEV₁ = 3/4 HFEV₁, and that negative lung damage expressed by uFEV₁ > HFEV₁ is theoretically impossible.

Since small airway damage accumulated over many years is the main driver for lung degradation in CF, age should be a good estimator of lung damage. I therefore plotted age against the lung damage computed using the above formula for every individual. I stratified the population by age groups to highlight underlying trend in the data. As expected, there is a clear increase of lung damage with age on Figure 1.4. The mean group's age rises from 44% in age group 18-30 years old, to 49% in age group 30-40 and 55% in age group 40-50. I ignored the age group 50-66 because i) very unhealthy individuals that might lie in the previous age groups would most probably, and unfortunately, not have reached such an old age; ii) the statistics based four individuals are not reliable. I compared the means, and not other quartiles, because the spread of the box-plots is more indicative of the size of the group than the variability of the data.

Fig. 1.4 Relationship between permanent lung damage approximated from the data and age. One can observe a clear increase of lung damage with the mean group's age from 44% in age group [18-30), to 49% in age group [30-40) and 55% in age group [40-50)



Identifying small airway blockage in the data

Using the same definition of unblocked FEV₁ as in the previous section, I can formulate an estimator for the small airway blockage as a ratio of FEV₁ and unblocked FEV₁:

$$\left(1 - \frac{FEV_1(L)}{uFEV_1(L)}\right) \cdot 100 \quad (1.2)$$

Since an acute pulmonary exacerbation is generally linked to a temporary increase in small airway blockage (excess mucus production), I used the exacerbated labels from Damian's predictive algorithm (cite X) to indicate the presence of small airway blockage. I plotted the results in Figure 1.5, where each vertical bar contains the FEV₁ records for a single individual. I expect measurements performed in an exacerbated period (red) to have a higher small airway blockage than measurements performed in a stable period (blue). I have three

Fig. 1.5 Relationship between the small airway blockage approximated from the data and the exacerbation labels from the predictive classifier in [?]. One bar is one individual, the results are presented in Table 1.1

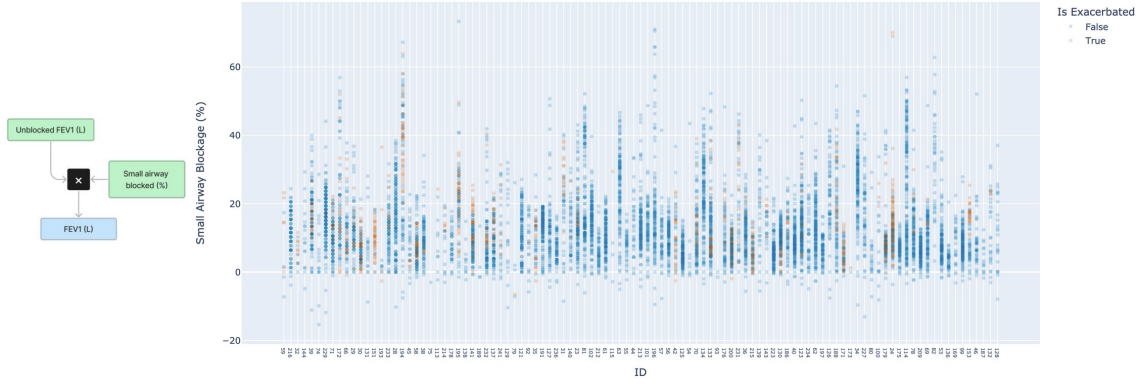


Table 1.1 Results of grouping individuals in Figure 1.5 with similar behaviours. The majority of the individuals have a higher small airway blockage during exacerbations. It confirms that exacerbations tend to correlate with small airway blockage.

| # | Case Observed | Individuals (Total: 96) | Expected? |
|---|---|-------------------------|-----------|
| 1 | Exacerbated labels above stable labels | 27 | Yes |
| 2 | Exacerbated labels mixed with stable labels | 13 | Yes |
| 3 | Exacerbated labels below stable labels | 2 | No |
| 4 | Too few exacerbated labels | 47 | Yes |
| 5 | Too few points | 9 | Yes |

remarks about this figure. Firstly, although the labeling is binary, going from stable to exacerbated is, in reality, a progressive change. Measurements done at the boundary of the stable/exacerbation period can be noisy. I therefore removed the datapoints located at the periods of transitions between exacerbated and stable states, as explained in section X. Secondly, very sick individuals under chronic inflammation are permanently exacerbated. As such, there might not be much difference between the clinical symptoms during an exacerbation and during a stable period. In this case the red/blue points can be mixed without a clear ordering. Thirdly, the labels are not very informative for individuals that have mostly one colour. I decided to keep them, though, to show a transparent picture of the CF population from the SmartCare study.

I summarised my observations in Table 1.1. Among the individuals with enough labels, 65% of the individuals show a higher small airway blockage in an exacerbated period (case 1), 30% have an unordered mixture of labels (case 2), and 5% are unrealistic examples with a lower small airway blockage in exacerbated state (case 3).

In conclusion, these two visualisations (figure 1.4 and figure 1.5) confirm that the multiplicative factor is a meaningful way to express the relationship between the healthy FEV₁, the airway resistance, and the observed FEV₁ respective to the data.

1.3 Conditional probability tables

In section X and X, I have defined and validated the graphical representation of the FEV₁ side of the model. I will now explain how I encoded the medical knowledge into the three factors from Figure 1.2, namely: the healthy FEV₁ prior (F1), the multiplicative factor (F2), the noise factor (F3). As explained in section X, I decided to discretise every variable by a sum of piecewise uniformly distributed random variables. Consequently, the factor functions are represented conditional probability tables (CPTs) instead of continuous conditional probability density functions. The dimensionality of a CPT is given by the cardinality of the variables connected to the factor.

1.3.1 Modelling an individual's healthy FEV₁ prior

To compute the healthy FEV₁ prior, I implemented the reference equations for normal lung function introduced in section X. It was more difficult than expected because the paper does not explicitly states how to quantify the uncertainty around the FEV₁ value predicted by their fit, which I need to derive a probability distribution for that FEV₁ value. I contacted the Global Lung Initiative (GLI) to get additional documentation and will hereby how I established a mapping that assigns a probability to any given healthy FEV₁ value.

The GLI performed a regression on their FEV₁ data drawn from a large-scale healthy population study. They used a generalised additive model for location, scale and shape (GAMLSS) using three parameters (height, age, and sex). I found in the supplementary documentation the function to compute the lower limit of normal - the threshold below which FEV₁ values are considered pathological (equation 1.3). By changing the standard score, this function can give the location of the percentile, corresponding to the selected standard score, on the FEV₁ axis. Note that the location (M), shape (S), and skewness (L) coefficients can be read or interpolated using the referred tabular data (cite X).

$$\text{FEV}_1 = f(\text{z-score}) = \exp\left[\log(M) + \frac{\log(1 + \text{z-score} LS)}{L}\right] \quad (1.3)$$

I then inverted this function to be able to get the standard score for a given FEV₁ value. Since healthy FEV₁'s PDF is approximated by a piecewise constant function, I could then integrate

the inverted function over the relevant bin of healthy FEV₁ to obtain the standard score for that bin. Lastly, I could read the probability associated to the standard score on the normal distribution. The steps are summarised in the block of equations below.

$$\begin{cases} \text{z-score} = f^{-1}(\text{FEV}_1) = \frac{1}{S \cdot L} \exp\left(L \log\left(\frac{\text{FEV}_1}{M}\right) - 1\right), \\ \overline{\text{z-score}} = \int_a^b f^{-1}(\text{FEV}_1) d(\text{FEV}_1), \quad \forall \text{FEV}_1 \in [a, b], a, b \in \mathbb{R}_+, \\ P(\text{FEV}_1) = \frac{1}{\sqrt{2\pi}} \exp\left(-\frac{(\overline{\text{z-score}})^2}{2}\right). \end{cases} \quad (1.4)$$

Figure X shows an example of a healthy FEV₁ given a specific individual.

1.3.2 Multiplicative factor to encode P(FEV₁ | healthy FEV₁, airway resistance)

The factor F2 on figure 1.2 is a reducing factor whereby the healthy FEV₁ gets multiplied by the airway resistance to produce the underlying FEV₁.

$$uecFEV_1 = HFEV_1 (1 - AR) \quad (1.5)$$

To encode this relationship into a CPT, I have used the convolution equation and the discretisation method respectively introduced in sections X and Y. To simplify the notation and for generalisation purposes, I have substituted *uecFEV₁* by *Z_C*, *HFEV₁* by *X_C*, and $(1 - AR)$ by *Y_C* for the rest of the section. Using the discretisation from section X, I can write:

$$X_C = \sum_{i=1}^n X_{D_i}, \quad \text{where } X_{D_i} \sim \mathcal{U}(x_i, x_{i+1}), i \in [1; n] \quad (1.6)$$

Similarly, *Y_C* and *Z_C* are discretised into *m* and *q* uniformly distributed variables. I can therefore express *Z_C* as following:

$$\begin{aligned} Z_C &= X_C Y_C \\ &= \left(\sum_i X_{D_i}\right) \left(\sum_j Y_{D_j}\right) \\ &= X_{D_1} Y_{D_1} + X_{D_1} Y_{D_2} + \cdots + X_{D_1} Y_{D_m} + \cdots + X_{D_n} Y_{D_1} + \cdots + X_{D_n} Y_{D_m} \end{aligned} \quad (1.7)$$

Z_C is a series of bin-wise multiplications of uniformly distributed random variables. The contribution of each term to the PDF of *Z_C* can be computed by convolving *X_{D_i}* with *Y_{D_j}*

multiplicatively (section X):

$$P(Z_C | X_{D_i}, Y_{D_j}) = f_{X_{D_i} Y_{D_j}}(z) = \int_{-\infty}^{\infty} \frac{1}{|y|} f_{X_{D_i}}(z/y) f_{Y_{D_j}}(y) dy \quad (1.8)$$

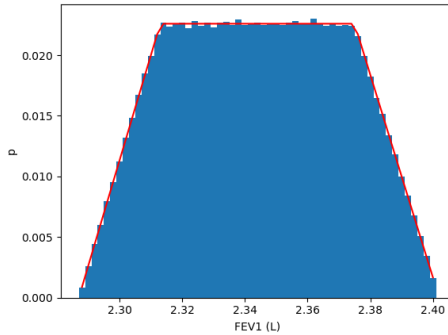
I had to derive the analytical solution of this equation by hand (see appendix A) because I could not find solutions for multiplicative convolutions in literature even in the relatively simple case of uniformly distributed random variables (literature mainly covers additive convolution). The solution writes:

$$P(Z_C | X_{D_i}, Y_{D_j}) = \begin{cases} \log\left(\frac{z}{x_i y_j}\right) & \text{for } x_i y_j \leq z \leq x_i y_{j+1} \\ \log\left(\frac{y_{j+1}}{y_j}\right) & \text{for } x_i y_{j+1} < z < y_j x_{i+1} \\ \log\left(\frac{y_{j+1} x_{i+1}}{z}\right) & \text{for } y_j x_{i+1} \leq z \leq x_{i+1} y_{j+1} \end{cases} \quad (1.9)$$

The above is defined when $x_i y_{j+1} \leq y_j x_{i+1}$. If this inequality does not apply, swap X_D with Y_D and solve the same equation.

I validated my derivation in the appendix against a sampling approximation, see figure 1.6.

Fig. 1.6 Analytical solution (red) against sampling solution (blue) to the multiplication of two uniformly distributed random variables. Example for healthy FEV₁ in the range 4.40-4.45 L and airway resistance in the range 44-46%. With $FEV_1 = HFEV_1 (1 - AR)$, the resulting FEV₁ is indeed defined from 2.288 to 2.403 L



For each bins i and j of the parent variables, I redistributed the resulting PDF from figure 1.6 into the bins of the child variable. The conditional probability table can therefore be computed, up to a normalisation constant for the edges, as follows:

$$\forall k \in [1; q], i \in [1; n], j \in [1; m],$$

$$CPT_{k,i,j} = P(Z_{D_k} | X_{D_i}, Y_{D_j}) = \int_{z_k}^{z_{k+1}} f_{X_{D_i} Y_{D_j}}(z) dz$$

Since I integrated over the valid range, the probabilities outside the range will be truncated during the normalisation.

1.3.3 Modelling the variability in FEV₁

Motivation to model the variability in FEV₁ A forced expiratory test is hard to reproduce because effortful to perform. This leads to outliers down. To palliate this effect, individuals are requested to make three consecutive blows of which the best performance is recorded (section X). However, I could still observe many outliers down on the longitudinal profiles. This suggests that individuals might not follow the protocol when performing spirometry at home, or that in some cases none of the three blows are representative of the underlying FEV. I have therefore applied a effort correction filter to the longitudinal profiles (section X). I purposely defined the filter to correct largely outlying values. The filter is conservative because it prefers to leave some noise to ensure keeping all the signal rather than remove all the noise with some signal.

The longitudinal profiles corrected for effort still display much day-to-day variability (Figure X). This variability can be caused by signal variation (a change of the health state of the lungs) or by non-pathological variations. In the later case, there are sources of variability in the longitudinal FEV data that are not related to effort, and that therefore are not addressed by the effort correction. When developing this model, I am concerned to not mistake normal biological variability and measurement noise for signal when inferring the airway resistance. I have therefore introduced a model of the FEV₁ variability to represent the factor function F3, i.e. the relationship between the effort corrected FEV₁ and the underlying FEV₁. To build this model, I first designed a filter to extract the measurement variability from the longitudinal profile using the difference in the characteristic time-scales of the variations in lung health and natural variations.

Measurement value decomposition

The model is based on a signal to variability segmentation of each measurement:

$$\text{measurement} = \text{signal} + \text{variability} \quad (L)$$

$$\text{variability} = \text{measurement} - \text{signal} \quad (L)$$

I considered that the variability is a function of a) the natural biological variations (e.g. recording time, circadian rhythm's influence), and b) the stochastic error of the measurement device. Hence, the variability most probably follows a gaussian distribution with patient- and

instrument-specific parametrisation. The signal contains a) the underlying FEV₁ value as well as b) the systematic error of the measurement device (potential calibration offset and nonlinearities). From this point of view, the time-scale of non-pathological variations is of the order of a small number of days, with sharp amplitudes; and the time-scale of signal variations ranges from daily to more than monthly, with often progressive changes over time.

Algorithm to filter the measurement variability

Similarly to the approach in my previous work (cite X), the method takes advantage of the difference between the time-scales of the non-pathological variability from the signal to separate them. For that the algorithm uses the same approach for each patient. For each entry, the algorithm first calculates a variability-free baseline by applying a mean filter to that entry's measurement value and its neighboring values. Although I explored more advanced methods (such as smoothing splines using de Boor's approach [see [?] or cite X]), I ultimately chose not to implement them, as it would have been difficult to offer clinicians a clear rationale for the chosen parameters. As the mean filter traverses the dataset, the resulting reference measurements form a smoothed version of original measurement time series. The algorithm then calculates residuals by subtracting each actual measurement from its corresponding reference measurement. A residual's value reflects the variability for that specific entry. Finally, by combining all patients' residuals, the method constructs a residual sample that provides an empirical basis for estimating FEV₁ variability (e.g., by computing standard deviations or percentile-based metrics).

The moving mean has two parameters. The window sets the number of days before and after the entry's date on which the mean filter is applied. The threshold defines a condition on the minimum number of measurements within the time window that is required to take the reference measurement as valid.

Building the variability model from the measurement variability

I used the same optimal parameters as in cite X to apply the algorithm: a window of 21 days with at least 7 days within that window to validate the data-density constraint. By running the algorithm on the FEV₁ records from the Breathe data-set, I obtained a set of residuals, that represent the variability unrelated to the evolution of lung damage, of which I computed the individual-level average variability, see Figure X.

To build the factor F3 (Figure X), I have to estimate $P(ecFEV_1|uFEV_1)$. I assumed that the variability was the same for every individual. From the introductory section about noise modelling (section X), the technical noise from the measurement device is typically

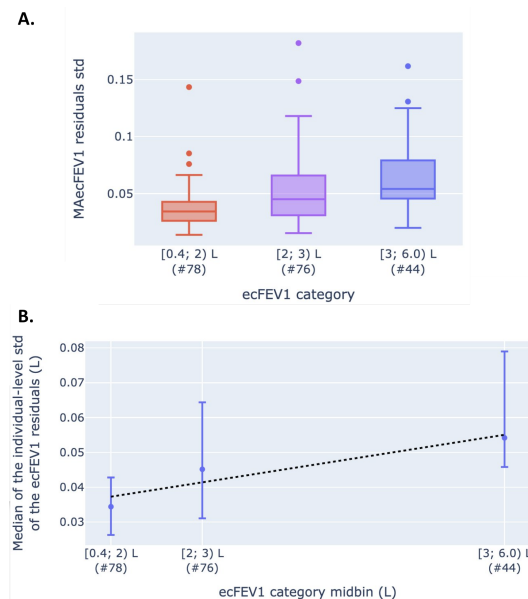
additive and gaussian. A simple factor would therefore be to use an additive gaussian noise, centered on the underlying FEV_1 and with the standard deviation taken as the median over the population (on the boxplot from Figure X).

However, the previously-mentioned signal-dependent variability related to the natural biological variations is typically multiplicative (section X). I therefore produced a plot of the effort corrected FEV_1 versus the individual-level variability to evaluate how wrong the additive noise hypothesis would be. To extract the trend from the set of datapoints, I grouped the $ecFEV_1$ in three categories with a balanced amount of individuals per category, see Figure 1.7 A. If the additive noise hypothesis was a perfect predictor of the variability, then the categories would have the same median values. Since it is not the case I decided to add a multiplicative dimension to the model of the FEV_1 variability such that:

$$ecFEV_1 \sim \mathcal{N}(uFEV_1, a uFEV_1 + b) \quad (1.10)$$

I performed a regression with least squares to evaluate the best matching parameters a and b , see Figure 1.7 B.

Fig. 1.7 Variability model to encode $P(ecFEV_1|uFEV_1)$. A shows that the individual-level std of the $ecFEV_1$ residuals' increases with $ecFEV_1$. This justifies using a gaussian model with an additive and a multiplicative component: $\mathcal{N}(uFEV_1, a uFEV_1 + b)$. B shows the result of the regression going through the mid-bin of each group, hereby setting the gaussian noise parameters to $a=0.00510174$ and $b=0.03032977$



1.4 Characterising the health of the respiratory zone with oxygen saturation

Oxygen saturation is routinely employed across a wide range of respiratory conditions, especially in case of hypoxemia that might require an immediate oxygen therapy (section X). It is however not generally used to monitor mild or moderate symptoms in lung health. Healthy lungs can tolerate considerable damage before oxygen starts to decline which means that oxygen saturation is a strong indicator of severe lung damage but it is a weak indicator of mild or moderate lung damage. As explained in section X, this redundancy is due to the nonlinearity between PaO_2 and SpO_2 in the hemoglobin dissociation curve and to the biological mechanisms that compensate for reduction in PaO_2 . Unlike FEV_1 for the conducting zone, selecting oxygen saturation to assess damage in the respiratory zone was therefore not an obvious choice. Nevertheless, it is important to not dismiss it if there might be value in using it. For example, the patterns observed in Figure 1.1 are encouraging as they suggest that subtle fluctuations amidst the variability in oxygen saturation measurements (the normal range is 95-100%), ignored in clinical practice, can be identified. Additionally, unlike DLCO test and PaO_2 measurements that would provide a more direct assessment of the lung's ability to exchange gas, oxygen saturation is a non-invasive measure, requiring a small and inexpensive electronic device (section X). It therefore respects the project's aim to model lung health with easily collectible data.

I have faced three main challenges in this section. The first one was to separate the normal from pathological variability in oxygen saturation. The second challenge was to identify whether a drop in oxygen saturation is caused by an issue in the conducting zone, the respiratory zone, or both. The third challenge was to understand if it is possible to identify moderate lung damage using the second order signals in the oxygen saturation data. Resolving the third challenge would be interesting because subtle signals in oxygen saturation have not been explored in literature.

In this section, I present a comprehensive theoretical and data-driven analysis of oxygen saturation. I develop a model that can extract these signals to provide lung health insights that go beyond the conventional use of oxygen saturation in clinical settings.

1.4.1 Structuring the relationship between oxygen saturation and lung health using physiology knowledge

Due to the natural fluctuations in oxygen saturation (section X) and the demographic difference between men and women (section X), a healthy individual's hemoglobin does not

always carry its maximum oxygen capacity. Consequently, to use oxygen saturation as a marker of lung damage, the model has to be able to separate which proportion of oxygen decrease is pathological and which proportion is not. Hence, I adopted the same approach used for FEV₁ to design the model structure (section X). I introduced a healthy baseline and a noise model to correct for the non-pathological sources of uncertainty in oxygen saturation.

Healthy oxygen saturation The HO2Sat variable is the healthy baseline that is personalised to an individual - it hereby corrects for the individual-level variability in oxygen saturation. I estimated its prior distribution by performing a regression based on the population's demographic parameters, of which sex is already known from the literature study (section X). Realisations from this random variable represent baseline oxygen saturation values for an individual, i.e. values that would be expected if this individual did not have any lung degradation.

Underlying oxygen saturation The "noise" model addresses the measurement-level variability. This variability rises from the oximeter's technical noise and the natural biological variations in oxygen saturation (section X). I have introduced the underlying oxygen saturation (uO2Sat) variable to represent the oxygen saturation corrected by those two sources of uncertainty.

O2SatFFA to split damage between the conducting and respiratory zones As a consequence of the high redundancy in the lungs (section X), any drop from the baseline oxygen saturation implies a significant compromise in oxygen transport. In section X, I opted to study the lungs by distinguishing two broad regions instead of looking at the airway generation continuum. The model therefore need only determine whether a pathological variation in oxygen saturation stems from one region (the conducting zone) or the other (the respiratory zone). I introduced a variable, oxygen saturation if fully functional alveoli (O2SAtFFA), to split the damage between those two regions, assuming they can influence oxygen saturation levels. I will justify this assumption in section X when looking at the data. According to the pathway of oxygen flow in the lungs, a decrease in oxygen saturation would first be attributed to high airway resistance and then to significant alveolar damage. O2SatFFA therefore represents the drop in oxygen saturation from a healthy baseline caused by increased airway resistance.

Inactive alveoli to characterise the health of respiratory zone Further drop from O2SatFFA must be due to causes other than airway resistance, be it i) any form of alveoli

blockage or damage that impairs gas exchanges (e.g. mucus blockage, reduction in diffusion through the membrane due to thickened blood-gaz barrier, damage due to chronic inflammation), or ii) remaining small airway blockage not captured by the airway resistance. The later is related to the fact that only significant damage in the small airways is reflected by FEV₁, as seen on the airway generation contribution to airway resistance curve in section X. I introduced the inactive alveoli (IA) variable, which represents the proportion of drop in oxygen saturation that is caused by the two above-mentioned sources of oxygen transport impairment.

To conclude, I extended the graphical representation of the model from figure 1.2 with the variables introduced in this section, as can be seen on figure 1.8. I also added the factors to connect the variables. F4 represents the prior for the healthy oxygen saturation (HO2Sat). F5 and F6 are reducing factors: they quantify the amount healthy O₂ saturation gets reduced, firstly by airway damage and secondly by alveoli damage (and remaining small airway blockage not reflected by the airway resistance), to obtain the O₂ saturation measurement. O2SatFFA is the intermediary variable which accounts for the damage in the airways but not in the alveoli. After the two step reduction we obtain the uO2Sat. The noise model simulates the technical noise and the daily biological variations that explain why for a single uO2Sat value, multiple O2Sat values can be measured with an oximetry test. I will justify the choice of the factor functions in the next section.

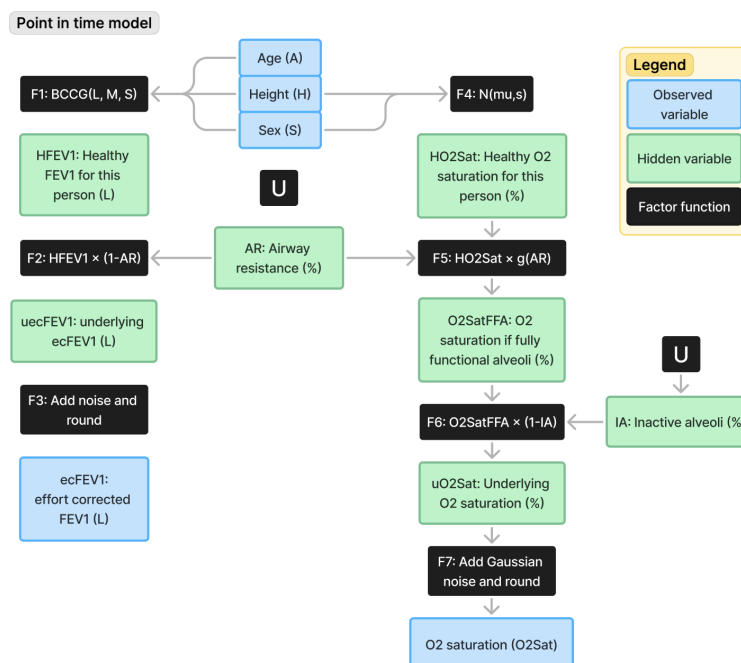


Fig. 1.8 Model structure with the FEV₁ and the oxygen saturation side (extension from 1.2

1.4.2 Data validation of the oxygen saturation side of the model

In this section, I will validate the model structure presented before by thoroughly studying the data from the CF studies. Additionally, I have stated that F5 and F6 are reducing factors, but I have not yet explored the exact relationship between the neighbouring variables for each of those factors. Unlike the FEV₁ side of the model where even the nature of the factor F2 could be chosen by the physiological understanding of what FEV₁ measure, I have not found documents in literature to explain the physiological relationships between oxygen saturation, airway resistance, and alveoli damage. This probably stems from oxygen saturation being used to alert of extreme ventilation-perfusion mismatch, rather than for in depth continuous health monitoring. Hence, this part of the project is quite exploratory work. I have therefore progressed step-by-step and carefully analysed the data to challenge the model structure and define the nature of the factor functions F5 and F6.

CF pathophysiology is marked by long-term lung damage from progressive small airway disease and by short-term, reversible fluctuations in airway blockage. To motivate the study of how oxygen saturation relates to lung health, I formulated hypotheses to see whether these two forms of lung damage are identifiable in oxygen saturation data. This allows to evaluate the extent to which oxygen saturation can inform our understanding of lung health.

I set hypotheses for how small airway blockage, represented by exacerbated labels in the data, affect oxygen saturation.

- HP1.1: O₂ is affected during exacerbations, at least for some individuals or exacerbations.
- HP1.2: O₂ is affected during the onset of an exacerbation but is corrected for by the body even before the exacerbation is resolved, for example on a time scale of a week or faster, at least for some individuals or exacerbations.
- HP1.3: O₂ is unaffected by exacerbations. This hypothesis can already be disproved, at least at population-level, because of the distribution shift on the SpO₂ density plot from Figure 1.1.

I also set hypotheses for how long term lung damage, represented by the signal during stable periods, affects oxygen saturation:

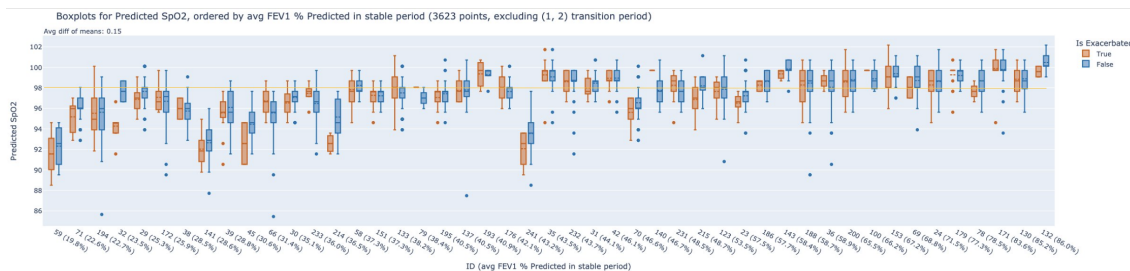
- HP2.1: O₂ is affected by long term lung damage, at least for some individuals.
- HP2.2: O₂ is unaffected by long term lung damage.

Then, I defined hypotheses to challenge the correctness of the model structure from Figure 1.8, with the two sequential reducing factors.

- HP3.1: O₂ is affected by airway resistance for individuals that have an advanced airway disease
- HP3.2: O₂ is affected by alveoli damage

To explore those hypotheses, I produced, on Figure 1.9, a visualization of the predicted oxygen saturation during exacerbated and stable period from left to right by individuals with increasing marker of CF small airway disease severity. I used the SmartCare CF data set to have access to the exacerbation labels from Damian's research project (cite X) of which I excluded transition periods to improve confidence in the labels (section X). Furthermore, given that reduction in oxygen saturation occurs only in extreme cases, using the SmartCare dataset with individuals who are sicker than those in the Breathe study increases the likelihood of observing clearer, more pronounced signals in the relationship between lung damage and oxygen saturation. On the plot's x-axis, I used the average FEV₁ in percent predicted during the stable period as a proxy for disease severity. On the y-axis, I computed the oxygen saturation in percentage predicted after correcting the measurements for the sex bias described in section X. Concretely, I divided women's measurements by X%, and men's by X%, which means that the threshold for normal oxygenation, as shown with the green line, is shifted upwards to 97-98% instead of being at 95%.

Fig. 1.9 Visualisation of the predicted oxygen saturation during exacerbated and stable period for every individual, ordered by an overall measure of CF small airway disease severity. I added the mean, highlighted by the dotted line, on the boxplots. The green horizontal line shows the limit for normal SpO₂ adjusted to after the correction by the sex bias.



Validating that oxygen saturation is sensitive to different aspects of CF pathophysiology

I will now study the figure in regard of the relationship between oxygen saturation with reversible small airway blockage (HP1.1-3) and permanent long term lung damage (HP2.1-2).

On Figure 1.9, there are three categories of individuals

1. For the vast majority of individuals, the mean of the red box (records made during an exacerbation) is lower than the mean of the blue box (records made during a stable

period) by one to three percentage points. This confirms that manifestations of an acute pulmonary exacerbation in the small airways of CF individuals can affect oxygen saturation (HP1.1) and hereby rejects HP1.3.

2. Two reasons can explain the few cases where the means during exacerbated and stable periods are equal. The first one is healthy individuals with healthy lungs: an individual can have so few permanent lung damage that the additional damage produced during an exacerbation is still not enough to cause a desaturation in oxygen. The more to the right end of x-axis the individual is, the more likely this reason becomes. The second reason is healthy individuals with degraded lungs: an individual can have an amount of damage that puts themselves at risk of ventilation-perfusion mismatch during an exacerbation despite having no or few symptoms during stable periods. In this case, the compensatory mechanisms can kick in during exacerbations to maintain PaO_2 at a normal level thus preventing an oxygen desaturation (HP1.2). This rational is more likely for the sicker individuals on the left-side of the plot. Consequently HP1.2 remains plausible albeit without a high level of confidence due to having only X examples in the data available.
3. Individuals with a higher mean oxygen saturation during an exacerbated period might be due to true positives and false positives miss-classifications by the predictive algorithm (as shown in Figure 4.5 of the thesis report cite X).

The impact of long-term damage on oxygen saturation can be assessed by analysing the trend in predicted SpO_2 during stable periods (blue boxes). Looking at the top envelope of the data created by joining the boxes' top values, oxygen saturation decreases at population-level when going from right to left: on the right all blue boxes are above the green line, whereas on the left all the boxes are below it. I have already mentioned this effect in the analysis of figure 1.1 in section X. This suggests that the long term lung damage has an impact on oxygen saturation, i.e. HP2.1 would valid while HP2.2 could be rejected.

Validating that airway resistance and inactive alveoli have an impact on oxygen saturation I have hereby confirmed that oxygen saturation is sensitive to small airway blockage as well as long-term lung damage. I then aimed to challenge the factors structure by looking at the data and test the third family of hypotheses.

In CF alveoli damage comes as a result of cumulative small airway damage. Alveoli damage and airway damage are, inherently to that process, intricate. Hence, it will be difficult by analysing CF data to differentiate damage coming from one or the other regions of the lungs. I will explain later how having access to additional data from other obstructive lung

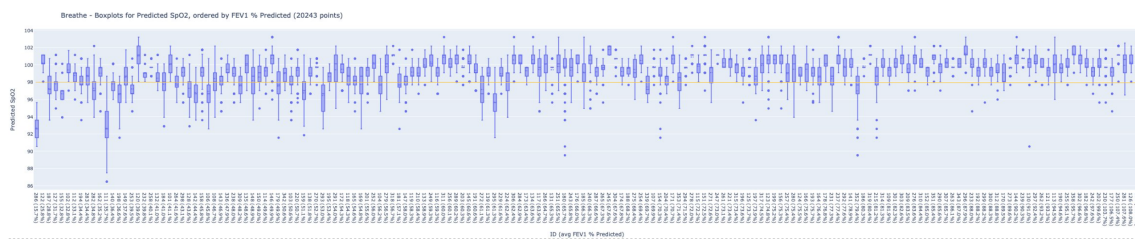
diseases would help fully unmix them. In the meantime, I describe how I managed to partially differentiate airway resistance and alveoli damage with the CF data at my disposal.

With this challenge in mind, it is therefore crucial to understand whether it is alveoli damage or airway resistance, or both that are involved in the oxygen saturation reductions highlighted by the vertical spread of the boxplots on figure 1.9.

First, I will illustrate that airway resistance affects oxygen saturation by revisiting the “top curve” analysis, which confirmed hypothesis HP2.1. Here, the x-axis shows the mean FEV₁ (in percent predicted) which is highly correlated with the airway resistance from the FEV₁ side of the model. Because a reduction caused by alveolar damage would not be reflected in spirometry, the observed downward trend demonstrates that airway resistance is the sole predictor of the highest achievable oxygen saturation. Hence, this finding not only validates HP2.1 but, more crucially, supports HP3.1.

Since validating HP3.1 is crucial to have confidence in the factor graph structure drawn in 1.8, I decided to see if the patterns would be replicated on the Breathe data. I reproduced the visualisation on this new dataset, using the same computation for the axes, and adding the same green line for the lower limit of normal, as seen on figure 1.10. Among the most obvious observations on this data, i) there are X times more individuals and three times more records, ii) individuals I did much healthier than in smartcare, with less than 1/3rd having an average FEV₁ in percent predicted below 60% (compared to over 3/4th for smartcare), and iii) there are no distinctions between stable and exacerbated periods for this dataset leading to just one boxplot per individual.

Fig. 1.10 Visualisation of the predicted oxygen saturation during exacerbated and stable period for every individual, ordered by an overall measure of CF small airway disease severity. I added the mean, highlighted by the dotted line, on the boxplots. The green horizontal line shows the limit for normal SpO₂ adjusted to after the correction by the sex bias.



At first the signal is not very clear, which makes sense because I am studying a phenomenon that is not addressed in details in literature, and not expected to be seen by clinicians. Yet again, the green line also marks a separation between the right where almost all the datapoints lie above it, and the left where a large portions of the boxes are below it. The fact

that the same signal replicates on this new dataset strengthened my confidence that airway resistance indeed affects oxygen saturation (HP3.1).

On figure 1.9, why are the individuals that have the same average FEV₁ in percent predicted but different predicted oxygen saturation? The examples for individuals 35 and 241, and 39 and 141 suggest that with the same airway resistance, the one with a higher in oxygen saturation would have more damaged alveoli.

To summarise, given oxygen saturation measurement, the drop from its healthy baseline is caused by a mixture of airway resistance and alveoli damage, which are intricate in CF. In an attempt to distinguish between the two, I identified the "top" curve which is a clear marker of the influence of, solely, airway resistance. I have therefore decided to encode this "top" curve in F5 (see graph 1.8) as a deterministic factor function $HO2Sat \cdot g(AR)$ which, given an certain airway resistance compute the percentage of drop from $HO2Sat$. Given that the uncertainty on the variability of this relationship is difficult to study given the intricacies between small airway damage.

The intricacies between small airway and alveoli damage make it difficult to estimate the variability in this drop, or the error in the curve estimation. I therefore decided to fix $g(AR)$ as a deterministic function, thus pushing the rest of the uncertainty from F5 over to F6. F6 therefore includes the uncertainty in the SpO₂ drop due to i) alveoli that see airflow but that are damaged, ii) small airway blockage not captured by airway resistance, iii) underlying variability in F5.

Referring to individual 38 on figure 1.9 with this model, for a total SpO₂ drop of 4% on average, roughly 1% would be caused by airway resistance and 3% by inactive alveoli.

1.5 Conditional probability tables for the oxygen saturation side

In the previous section, I explained how oxygen saturation can be used to understand the health of gaseous exchanges. Then, I structured the model to estimate, given an individual, the airway resistance and the proportion of inactive alveoli by quantifying the reduction in oxygen saturation records from their "healthy" baseline. I defined and validated the structure (Figure 1.8) as well as the relationships between the variables. In this section, I will describe how I encoded the four factors (F4-F7) in the form of conditional probability tables. These factors are the heart of the model because they rule how a change in one variable will affect its neighbours (section X).

Also, from now on, I have only used the Breathe dataset because it is much richer than the one from Smartcare CF (section X), despite not having the exacerbated labels which were very informative to understand the relationship between oxygen saturation, FEV₁ and lung health (Figures X, Y, Z).

1.5.1 Modelling an individual's healthy oxygen saturation prior

The prior knowledge of the HO2Sat variable is the expected distribution of that variable "prior" to observing any model evidence. A good prior is a distribution that contains the true underlying value it is trying to predict, and is as narrow as possible. Unlike for FEV₁, there are no well established reference equations about the normal oxygen saturation in literature. I therefore decided to develop a custom equation based on the CF data-sets and elements from literature studies.

In its simplest form, I could model the HO2Sat prior by a random variable uniformly distributed in between 95% and 100%, the range of normal oxygen saturation (section X).

$$HO2Sat \sim \mathcal{U}(95, 100)$$

Although I am confident that the true HO2Sat would be contained in this prior, there is a lot of uncertainty because every value from 95 to 100 is equiprobable. I know, from my literature review, that oxygen saturation in healthy individuals is roughly between 96-97% for men, and 97-98% for women (section X). Hence, by observing the individual's sex, I can improve the simple model by increasing the probability around on the more commonly observed states for that sex. I will explain in the rest of the section how I implemented this and how I have tried to further narrow down the uncertainty in HO2Sat.

Numerous non-pathological factors can influence oxygen saturation. Altitude is probably the best-known cause of oxygen saturation drop because people can experience altitude sickness when trekking in the mountains. However, I excluded it - as all environment factors - because I aim to understand an individual's lung health with physiological information first. Also, I do not expect altitude to be very informative in the United Kingdom which is a relatively flat country. Amongst the individual metadata, the most interesting candidates to model an individual's HO2Sat prior were sex, lung size, and age.

Sex I found little mention in literature of physiologic characteristics responsible for difference in blood oxygenation. The only well documented influence factor is sex: oxygen saturation is typically higher in females than in males. The delta obtained is +0.7% in two studies, one on students, one on hospital patients/staff/visitors; and +1.4% in two other

studies mainly with student participants and with stricter exclusion criteria (section X). I find a 1% difference especially notable, given that normal range of oxygen saturation (95-100%) spans just over 6% of delta. Even more striking is that clinicians with decades of experience I spoke with were unaware of this sex-based bias. This could mean that the sex-bias in oxygen saturation is insignificant for clinical applications, in which case the initially suggested uniform assumption (Equation X) would suffice. From a scientific perspective however, the fact that such a substantial inter-individual variation has gone unnoticed by experts suggests that, with it, the model could uncover precious new insights into lung health.

Lung size I have reasons to believe that difference in lung size could lead to difference in baseline oxygen saturation. The lungs are subject to gravity due to their weight, which creates a pressure gradient from the top to the bottom of the lungs. Hence, under normal conditions, the lower regions of the lungs are exposed to higher pressures, which can affect the distribution of air and blood flow. In larger lungs, the total number of alveoli is higher, and gravity may influence the efficiency of ventilation differently depending on the regions of the lungs. For example, the lower regions might be less efficient in terms of ventilation-perfusion matching. Lung size might therefore impact on oxygen saturation.

Age With age, several physiological changes can impact oxygen saturation in the lungs. Reduced lung elasticity, decreased alveolar surface area, and weakened respiratory muscles make it harder for the lungs to efficiently exchange oxygen. Age-related changes in the cardiovascular system, such as decreased cardiac output and stiffening of blood vessels, can also hamper blood oxygen delivery throughout the body. Unfortunately, age is, in CF, an important marker of the progression of the disease. Having only CF data, I could not use age to model individuals with healthy lungs. Since I did not find a study of the relationship between age and oxygen saturation, I had to exclude age from the list of potential candidates.

To delve into the implementation, I wanted to see whether I could replicate the sex bias shown in O₂ saturation from literature on the Breathe data-set. Then I looked for a coorelation between oxygen saturation and lung size, which I approximated by the individual's predicted FEV₁.

I computed the correlation between an individual's maximum O₂ saturation value and height, predicted FEV₁ before and after correction by sex. I did this in a robust way by bootstrapping (2000 times with 90% sample size), thus obtaining in ranges instead of scalars. Since sex is a known bias in O₂ saturation (CITE), I corrected for it by normalising males and females measurement's by their respective mean and standard deviation. The results in

Table 1.2 Bootstrapped Pearson correlation coefficients between healthy O₂ saturation and lung size for 213 individuals. Healthy O₂ saturation is estimated by a robust maximum for O₂ saturation, defined as the individual's 5th highest measured value. Lung size is approximated by height and predicted FEV₁ and appears strongly and negatively correlated with O₂ saturation. After correction by sex, a strong evidence of weak correlation remains for height, but not for predicted FEV₁ as the range crosses 0.

| | Height | Predicted FEV ₁ | Height (sex corrected) | Predicted FEV ₁ (sex corrected) |
|--|---------------|----------------------------|---------------------------|---|
| Robust max of O ₂ saturation | [-0.2; -0.37] | [-0.15; -0.31] | [-0.06; -0.21] | [0.04; -0.11] |

Table ?? show strong evidence of strong linear correlation between O₂ saturation and height as well as predicted FEV₁. After correction by sex, only height remains correlated, although weakly, which indicated that sex the main explainer for the variability in O₂ saturation, and that height is a second order candidate. By curiosity, I also investigated the relationship with age, expecting it to naturally reduce as an healthy individual gets older. Running the bootstrapped correlation for age gave [-0.05; -0.2] both before and after correction by sex. This gives a strong evidence of weak correlation with O₂ saturation which is irrespective of sex. Even though age could have proven useful, especially if I had a dataset where age was not strongly linked to disease severity, excluding it did posed a risk of reducing the model's performance. However, because age appears to have only a weak correlation with oxygen saturation, omitting it likely will not significantly affect the model's accuracy. Hence, I defined healthy O₂ saturation as a linear function of sex and height.

$$HO_2Sat = a + b \text{ isMale} + c \text{ height} \quad (1.11)$$

I decided to use a linear regression to fit equation 1.11 and to optimise for least squares. Nonetheless, modelling the healthy O₂ saturation with a dataset of CF individuals is dangerous because the individuals are, by definition, not healthy. To minimise this risk, I chose to:

1. Run the regression multiple times, initially with all individuals and then by isolating a subset of increasingly healthier individuals, and plot the parameters' evolution. I used FEV₁% as the healthiness criteria as it is the most important metric to assess the lung health in CF care.
2. Validate the results against the literature studies performed on healthy populations. Since those studies only looks at the impact of sex and not height, I chose to first

correct for sex by fitting 1.12a, then for height by fitting 1.12b. This excludes the possibility of height capturing some of the relationship between O₂ saturation and sex, which would disallow the comparison against literature.

$$HO_2Sat = a + b \text{ isMale} \quad (1.12a)$$

$$HO_2Sat - a - b \text{ isMale} = c (\text{height} - \bar{\text{height}}) + d \quad (1.12b)$$

In equation 1.12b, centering height by its mean keeps the parameter d as close to zero as possible. This minimises the height's influence on the overall fit's intercept (a+d). In the results, d scaled like 10⁻¹⁵. I therefore did not plot it in the results on figure 1.11, and even removed it when implementing the model.

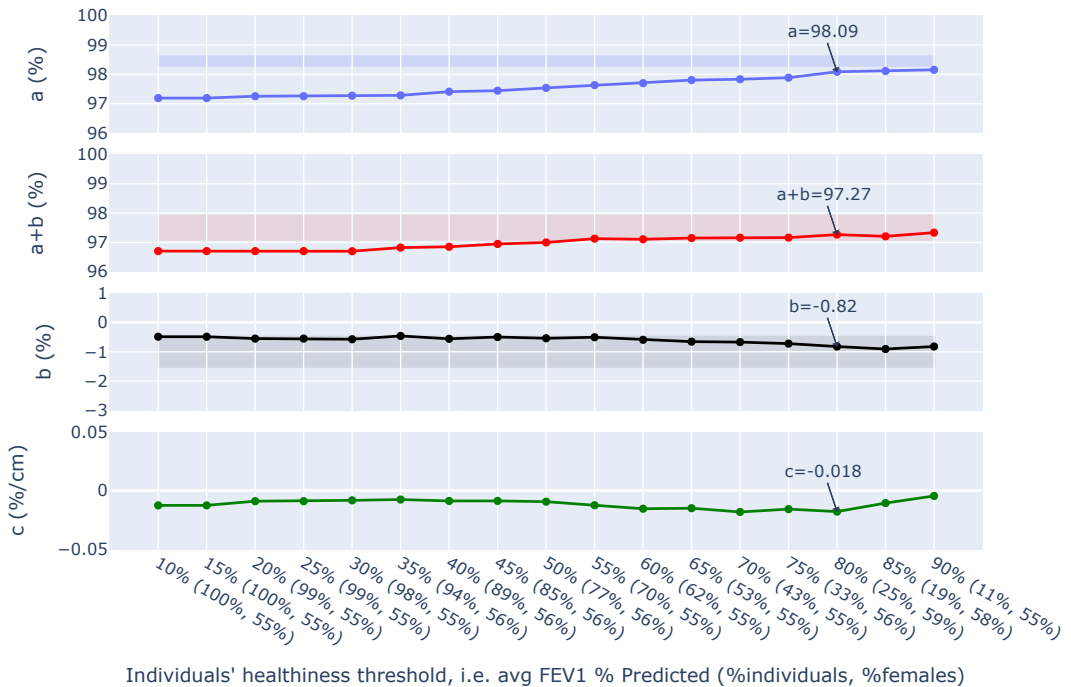


Fig. 1.11 Healthy O₂ saturation fit according to equations 1.11: evolution of the regression parameters with increasing individuals' healthiness threshold. The coloured rectangle represents range of values seen in healthy populations (CITE). The blue and red curves increase monotonically and, doing so, converge to values from literature after the 80% healthiness threshold. This indicates that the healthier the individuals, the higher the O₂ saturation.

Figure 1.11 shows that as the individuals' subset gets healthier (going from left to right), the height-related parameters converge to values from literature. I did not expect the fitted model to perfectly align with literature as the populations are different, especially as Breathe's participants have CF. Hence, this indicates that the healthiest CF individuals in the data-set are

representative of a truly healthy population, at least in terms of their O₂ saturation. Moreover, the parameters' values stabilise startgin from the 80% healthiness threshold, which I chose as the best choice to avoid excluding too many individuals. This choice is further comforted by clinical practice, where 80% FEV₁% is defined as the lower limit of normal for healthy populations (section X).

To include the uncertainty in the expected value, the model has to be probabilistic. Since the fit minimises the residuals' sum of squares, the healthy oxygen saturation can be modelled by a Gaussian distribution defined by:

$$HO_2Sat \sim \mathcal{N}(a + b \text{ isMale} + c (height - \overline{height}), RSE) \quad (1.13)$$

where I selected the parameters and computed the model's residual standard error (RSE) as follows:

$$\begin{aligned} a &= 98.09 \\ b &= -0.82 \\ c &= -0.018 \\ \overline{height} &= 166.55 \\ RSE &= 0.55\% \end{aligned}$$

Concretely, this model sets a baseline O₂ saturation of 98.1% for healthy females and 97.3% for healthy males. Then, the taller the individual, the smaller the healthy O₂ saturation becomes: every 10cm increase from the average height will reduce the baseline value by 0.2%.

1.5.2 The drop in oxygen saturation due to airway resistance

I have justified the reason for modelling F5, the drop caused by airway resistance by a deterministic function $g(AR)$, thereby leaving the uncertainty on the exact behaviour to the downstream factor F6. Having modelled the healthy prior, and the FEV₁ side of the model, I updated the visualisation from Figure 1.10 by plotting the airway resistance against the O₂Sat%, instead of the average FEV₁ in percent predicted against the oxygen saturation corrected by sex. I computed O₂Sat% by dividing each O₂ saturation measurement by the individual's HO2Sat (as developed in section X), by taking the distribution's mean. This removes the inter-individual non-pathological variability from the y-axis. It corrects for sex and height instead of just correcting for sex in Figure 1.10. To obtain the airway resistance, I ran belief propagation on the FEV₁ side of the model (developed in sections X and Y) for

each daily entry in the data-set, using the individual's age, sex, height, FEV₁ recorded on that day as model evidence. I used the discretisation parameters from table X (airway resistance is inferred in bins of X%). I computed the distributions' mean to get a point mass estimator for the inferred airway resistance. I thus obtained a set of airway resistance and O₂Sat% value pairs for each entry in the Breathe data-set, which I used to produce the updated plot on Figure 1.12.

The first element I will analyse on this figure is the curve traced by joining the highest points together (referred to as "top curve"), which indicates the maximum achievable O₂Sat%. It stays constant at low airway resistance, and then progressively decreasing as the airway resistance increases (ignoring the few high points around 50-60% which belong to only one individual). This suggests that the airway resistance is a predictor of the maximum achievable O₂Sat%. I had identified this when discussing HP3.1 by analysing Figure 1.10 in section X, except that the scatter plot provides clearer insight than the boxplots.

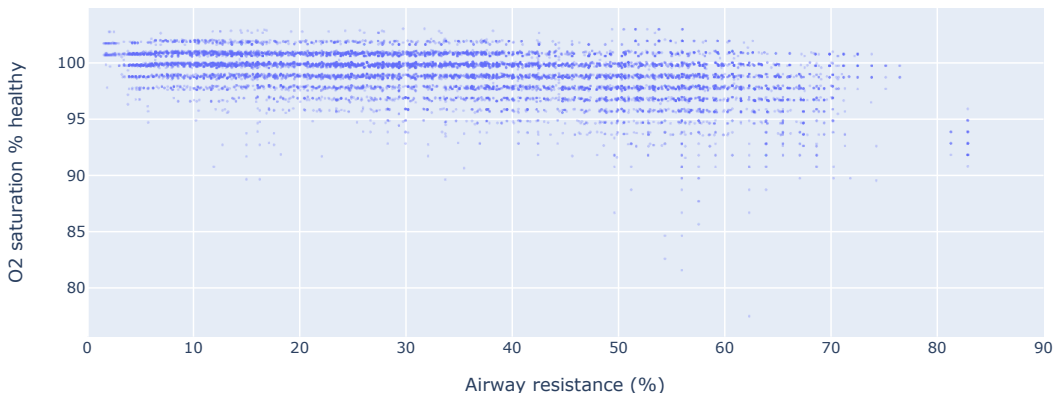


Fig. 1.12 Relationship between O₂Sat% and airway resistance. Values in 100-102% appear when O₂ saturation measurements are larger than their healthy values. This happens when the measured O₂ saturation is above its true value (due to measurement noise) or when the HO₂Sat value (taken as the distribution's mean) is below its true value, or a combination of both effects. The curve traced by the highest points, excluding the first 1-5 outliers, is roughly constant up to 40% airway resistance then it slowly decreases, with few data above 70%. Points are displayed with 30% opacity, which allows to differentiate one, two, and three or more superimposing points.

To understand what this maximum achievable O₂Sat% curve shows I will detail the underlying physiological mechanisms. The impact of airway resistance on healthy O₂ saturation is best understood by taking the example of asthma because it affects airway resistance exclusively (it does not affect alveoli blockage). In asthmatic individuals, O₂ saturation drops below normal levels, and sharply, only during severe asthma crisis where patients have to be moved to intensive care units and be put on oxygen REF X. O₂ saturation is otherwise

maintained within normal levels even though oxygen transport might be moderately impaired due to the natural compensatory mechanisms that maintain sufficient blood oxygenation (e.g. increased breathing rate and amplitude, blood redirection to ventilated regions of the lung, as explained in section X). Those compensatory mechanisms explain the saturating effect of O₂ saturation. On the hemoglobin dissociation curve (section X), as PaO₂ reduces from 100 to 60 mmHg, the SpO₂ remains roughly constant. However, passed 60 mmHg, the SpO₂ falls steeply.

I decided to encode the "top curve" in the factor F5 since it shows the impact of airway resistance. To extract this curve from the scatter plot on Figure 1.12, I performed the following steps:

1. I binned the airway resistance values in 2% wide intervals to increase the amount of data-points per bin while maintaining a high enough spatial resolution to fit a curve. The airway resistance initially had a 1% bin width due to the inference parametrisation.
2. I excluded bins with too little contributing individuals (<7) and data-points (<50) to prevent the extracted curve to overfit the data, see Figure 1.13 B and C.
3. Since O₂ saturation has a low signal to noise ratio I applied a robust maximum operator to each bin to retain a denoised version of the highest achieved O₂Sat% measurements, see Figure 1.13. For example, this removed the outlying values in the 50-60% airway resistance range that were specific to only one individual. I defined the robust maximum as the 80th-90th percentiles' average, which reads:

$$85^{th}rmax(\mathbf{x}) = \frac{1}{11} \sum_{n=80}^{90} prctile(\mathbf{x}, n)$$

4. I then ran a regression on the 85thrmax profile to obtain the optimal "top curve". I anticipated an initial constant phase where the airway resistance has no or little impact on O₂ saturation. In this phase, the lungs are healthy enough to maintain good ventilation with or without the need of compensatory mechanisms. Once a critical threshold is reached where the compensatory mechanisms are not sufficient to maintain normal PaO₂ (at roughly 40% airway resistance on Figure 1.12), then the SpO₂ starts to decrease continuously. To reflect medical expectation, I constrained the regression to a piece-wise constant and piece-wise polynomial function to the data by minimising

the residuals' sum of squares. The function reads:

$$f(x) = \begin{cases} x_0 \\ y_0 + k_1(x - x_0) + k_2(x - x_0)^2 + k_3(x - x_0)^3 \end{cases}$$

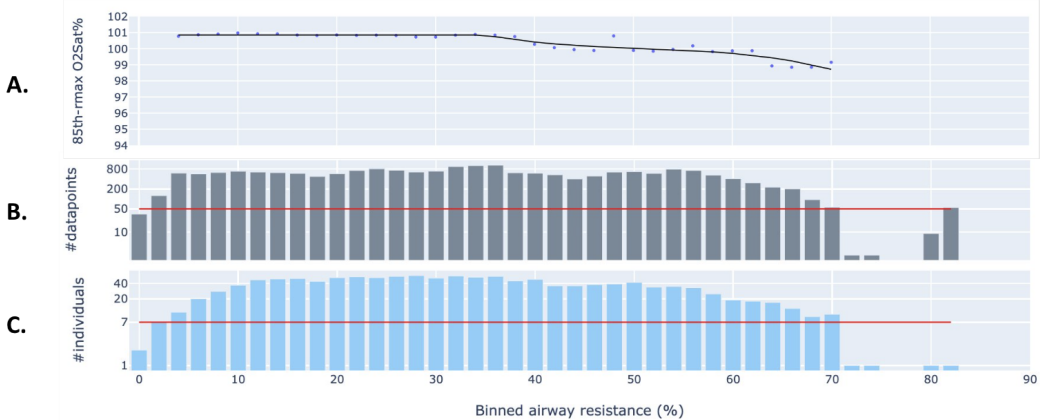


Fig. 1.13 Evolution of the maximum achievable O₂Sat% with airway resistance, and associated data scarcity. The fitted black curve (A) is constant up to 35% airway resistance, then slowly decreases until 70%. Past 70% of airway resistance too few data-points (B) with too few contributing individuals (C) were collected to draw a reliable curve.

Figure 1.13, shows the evolution of the maximum achievable O₂Sat% with airway resistance. I then used the fitted curve to define a multiplicative drop function $g(AR)$ to encode into the factor F5 such that $O2SatFFA = HO2Sat \times g(AR)$. I obtained the factor function on Figure 1.14.

To conclude, the multiplicative drop function on Figure 1.14 is a great achievement because validates clinical knowledge despite being drawn from bins with 7+ represented individuals and 50+ datapoints, and without applying any transformation to the O₂ saturation measurements from the data-set. In fact, the curve i) is constant for healthy airways (from 0% to 35% of airway resistance), ii) then it starts to decrease when airway resistance goes from 35% to 70%. At those values the oxygen's partial pressure is sufficiently reduced to enter the steep part of the hemoglobin dissociation curve, where O₂ saturation significantly desaturates, but the compensatory mechanisms kick in to maintain the O₂ saturation in normal levels. Above 70%, where I expected a sharp drop, the fit is unreliable as the airway resistance is too high to have allowed sufficient data collection, see plots B and C on Figure 1.13. In this region, individuals usually have to be put on oxygen.

Since this the model of the airway resistance's impact on healthy O₂ saturation validates clinical knowledge, it also shows that the FEV₁ side of the graph, used to infer the airway

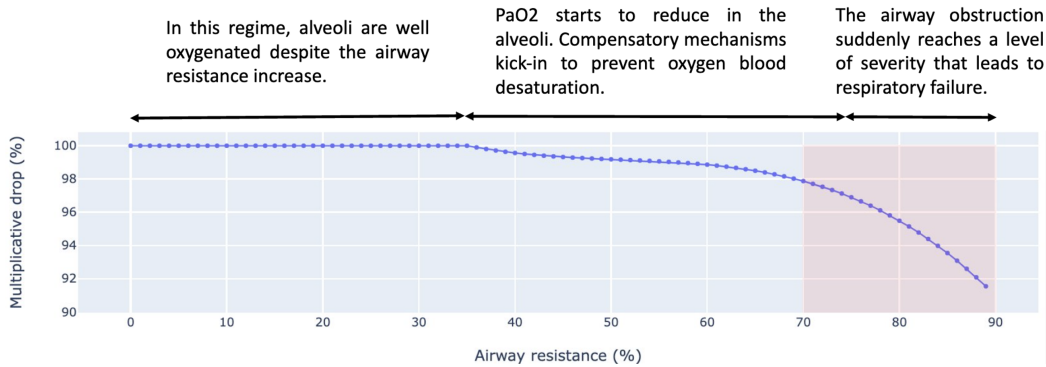


Fig. 1.14 Factor function F4: evolution of the multiplicative drop from healthy O₂ saturation with airway resistance. Three zones can be observed: 1) 0%-35% where airway resistance has no impact on healthy O₂ saturation, 2) 35%-70% where airway resistance reduces healthy O₂ saturation, and 3) above 70% where the fit is unreliable because of too few data-points.

resistance, and the healthy O₂ saturation's model are representative of the reality of the mechanisms that happen in the lungs.

1.5.3 Oxygen saturation noise model

When running an experiment, it is important to consider the noise in the data because it can bias the results. Specifically, the higher the signal to noise ratio (defined in section X), the more concerning the noise becomes. At first glance, Figure X shows that oxygen saturation seems to have a low signal to noise ratio, which makes it an important candidate for further noise analysis.

I expect three main sources of noise when performing an oximetry test. The first is the random technical noise of the oximeter (section X), which could differ from per oximeter (cite device noise comparison in background). The time of execution is the second source of noise, due to the natural biological changes that happen on the course of a day, e.g. the oxygen saturation typically reduces during sleep (cite X). The third source of noise is human, due how systematic the oximetry test is performed by the participant, which can vary for each participant and also for each test. I did not consider the participant-specific device calibration noise for the analysis because it is deterministic and would therefore even out when making the difference between two values. Although oximeter measurement noise assessment is extensively covered in literature, I could not find a reliable noise study that included the other types of noises. Hence, this is quite exploratory work.

I decided to model the factor F7, translating the relationship between O₂Sat and uO₂Sat, to reflect the behaviour of oximeters, which are subject to measurement noise and always

provide an integer result. The factor function linking O₂Sat and uO₂Sat contains two sequential components, as seen in Algorithm 1. The first component is a **Gaussian noise component**: the real value is shuffled according to a Gaussian distribution with the mean centered on that real value ($uO2Sat_{true}$) and the standard deviation (std_{gauss}), which has to be determined. The second component is a **rounding component**: the shuffled value ($uO2Sat_{noisy}$) is rounded to the nearest integer, thus producing the actual oxygen saturation measurement.

Algorithm 1 O₂ SATURATION Generative Noise Model

```

1: function GENERATEO2SATMEASUREMENT( $bin_{low}, bin_{up}, \sigma_{gauss}$ )
2:   Sample  $uO2Sat_{true} \sim \mathcal{U}(bin_{low}, bin_{up})$ 
3:   Sample  $uO2Sat_{noisy} \sim \mathcal{N}(uO2Sat_{true}, \sigma_{gauss})$ 
4:    $O2Sat \leftarrow \text{round}(uO2Sat_{noisy})$ 
5:   return  $O2Sat$ 
6: end function
```

To ensure the model reflects reality, its variance (var_{mod}) should equal the variance of the O₂ saturation measurements (var_{obs}):

$$var_{mod} = var_{obs} \quad (1.14)$$

Since the variance of the sum of two independent random variables is equal to the sum of their variance (cite X), I can decompose the model's variance into the two previously mentioned components, such that:

$$var_{mod} = var_{gauss} + var_{round} \quad (1.15)$$

By introducing the standard deviation, I can rewrite equations 1.14 and 1.15 to isolate std_{gauss} with respect to std_{obs} , which can be computed using from the data. It gives:

$$std_{gauss} = \sqrt{std_{obs}^2 - std_{round}^2} \quad (1.16)$$

I could also have derived std_{gauss} by computing the value of std_{round} and solve Equation 1.16. However, I chose to take an approach that focuses on the noise model as a whole rather than the characteristics of its components. I implemented the noise model from Algorithm 1 and determined std_{gauss} empirically to enforce the equality from Equation 1.14. I created the following a procedure:

1. Compute std_{obs} , the standard deviation of the O₂ saturation measurements for a typical healthy individual

- (a) Filter the healthiest individuals in the Breathe's data-set, i.e. the individuals with $\text{FEV}_1\% > 80\%$ (which is the lower limit of normal used in clinical practice cite X)
 - (b) Exclude individuals with less than 10 O_2 saturation measurements to mitigate the effect of potentially outlying values of standard deviations.
 - (c) Compute the standard deviation of the O_2 saturation measurements for each individual.
 - (d) Average the standard deviation across all individuals. This represents std_{obs} .
2. Determine std_{gauss} , the standard deviation of the noise model's Gaussian component
- (a) Initialise std_{gauss} according equation 1.16 with std_{obs} taken as the value computed in step 1, and std_{round} taken to 0.25. In fact, a rough estimate of the standard deviation of the rounding operation is one-quarter of the difference between consecutive reportable values [?]. In this case $std_{round} = 0.25$ since the uO2Sat's bin width is one percentage point.
 - (b) Sample one million points from the noise model (Algorithm 1, using uO2Sat in the bin [94.5-95.5]). I purposely take a bin far from the boundaries to avoid sampling outside of the uO2Sat's 50-100% range chosen when discretising this variable (see Table ??).
 - (c) Save the sample's standard deviation as std_{mod} .
 - (d) If $std_{mod} \neq std_{obs}$, manually update std_{gauss} to a more relevant value.
 - (e) Repeat steps 2.b-d until $std_{mod} = std_{obs}$

Running this procedure gave $std_{mod} = 0.9$ (the results of steps 1-3 are displayed in figure 1.15), and the equality in step 8 was validated for $std_{gauss} = 0.86$. I would like to point out that the initialisation criteria mentioned in step 4 was particularly accurate as it produced the exact same value ($\sqrt{0.9^2 - 0.25^2} = 0.86$).

Using this generative noise model, the conditional probability table of O2Sat given uO2Sat can be computed running Algorithm 1 a million times for each bin of uO2Sat, excluding results outside the uO2Sat range, and normalising to ensure that the sum of all the probabilities across O2Sat's bins equals one. Figure 1.16 shows the resulting O_2 saturation noise model can be used in both directions. In inference mode (Figure 1.16 A), I can be used to determine $P(\text{uO2Sat}|\text{O2Sat})$, the underlying distribution of O_2 saturation values given one measurement. The top-left histogram shows the Gaussian-shaped distribution of uO2Sat, which is expected given the mod Algorithm 1. At the boundaries, the distribution is half of a

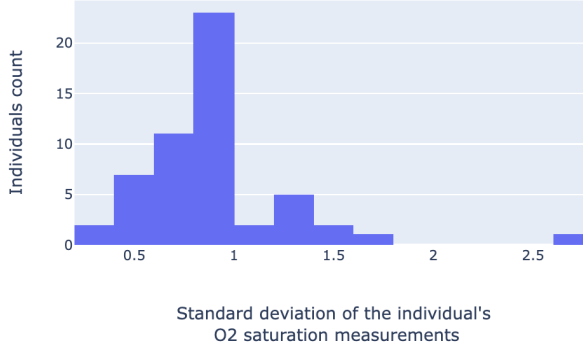


Fig. 1.15 Histogram of the standard deviation of O₂ saturation measurements for each Breathe's individual. The average standard deviation in this sub-population is 0.9. 54/213 individuals were included after applying the healthiness and the data density filters.

Gaussian distribution (see the bottom histograms). The standard deviation is smaller due to the border effects reducing the uncertainty in the measurements. The noise model can also be used in a generative mode (Figure 1.16 B) to obtain P(O₂Sat|uO₂Sat), the distribution O₂ saturation given a hypothetical uO₂Sat observation. The asymmetry in the top-right histogram reflects the asymmetry in the binning. In fact, only the right half ([95; 95.5]) of the full uO₂Sat interval contributing to O₂Sat ([94.5; 95.5]) is included. The distribution would be symmetrical if the two contributing uO₂Sat intervals were used ([95; 95.5] and [94.5; 95]).

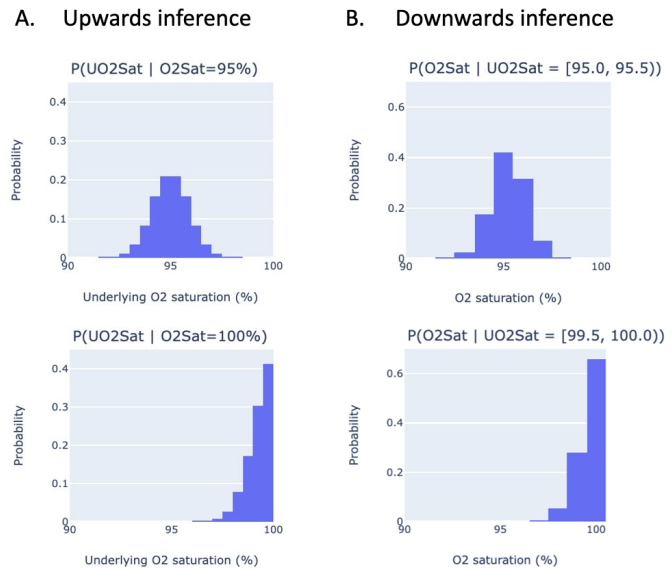


Fig. 1.16 Results of inference using the O₂ saturation noise model. The variables' discretisation parameters are set according to table ??.

1.5.4 Multiplicative drop in oxygen saturation due to inactive alveoli

The factor F6 is a reducing factor that expresses the drop from O₂SatFFA to uO₂Sat. It informs on the proportion of drop that is due to inactive alveoli. Unlike for the previous factors in this section that were fitted using elements of the Breathe data-set, this one is a mathematical operator. I computed the conditional probability tables for this factor using the same formalism presented for the factor F2 in section X, which was also a multiplicative factor.

1.6 A web-application for interactive inference

Previously in this chapter, I have designed a factor graph based on pulmonary physiology knowledge verified with signal in the data and I encoded the physiological behaviours in different methods into the factor functions. With the modelling part completed, I will now delve into running inference queries on the model to describe the various suspects of the lungs.

I've decided to build a web application for two main reasons: to show how a probabilistic graphical model of lung health can be used as a tool for communication between clinicians and patients, and also from a research perspective it allowed me to explore model behaviour understand how expected in our interpretable the results are ultimately validate and refine the model. The latter will be described in the next section.

In short, I have developed a fairly simple app as I put most research effort in model development. The app is intended to be used for a single individual. The first step is to reference the individuals clinical profile consisting of age 6 and height. This information will be used to compute the priors of HFEV₁ and HO₂Sat, referring to the implementation in sections X and Y. Secondly, the user can select model evidence, which are typically oxygen saturation and FEV₁, although I have also virtually allowed any variable to be observed for the purpose of scenarios testing. Thirdly, the user can use the sliders to set the model evidence to their measured or desired values. Instantly, in the background, the application runs an inference query to compute the posterior distribution of all latent (unobserved) variables. I have put an example of the user interface on figure X.

1.7 Model validation and usefulness

Probabilistic Graphical Model (PGM) Validation involves assessing how well the model represents real-world phenomena, which here translates into understanding whether it accurately

captures and generalizes the underlying data distribution of the CF population. Ultimately, a thorough validation not only supports accurate and trustworthy performance in real-world clinical settings but also fosters confidence among clinicians and patients who might use the model in clinical practice.

In this chapter, I did not have to validate the algorithms implementation because I I used an exact inference algorithm from an open source library (section X). I will first recall I performed step-by-step structural validation, then evaluate how the inference accurately describes the typical scenarios for a wide range of lung pathologies. Finally, I will show that the model correctly captures the distribution of lung health variability in the dataset it was built on without over- under-fitting.

1.7.1 Structural validation

Structural validation, as introduced in section X, involves using domain knowledge to ensure the choice of variables and their ordering makes sense. It also involves verifying the relationships between neighbouring variables.

I have performed the structural validation at each step of the model development, for example when I was evaluating if behaviours expected from pulmonary physiology knowledge where matched by signal in the dataset (sections X, Y, Z).

I also verified numerical and analytical solutions to CPT encoding against sampling (section X, X, X).

1.7.2 Domain expert inference evaluation and early diagnostic model capacity

Domain expert inference evaluation is a qualitative model validation. I have explained in section X, I can describe this model as computational representation of the medical mind map used by clinicians to reason on lung health based patient demographics and a pair of FEV₁ and O₂ saturation measurements. As such, the model is a correct representation of lung health if, given specific data inputs, the results validate clinical expectations from a doctor with extensive knowledge and clinical practice. That is a minimal requirement I have for the model capacities. From this perspective, if the model results is validated by domain expert, then it can be useful in practice to provide insight to patient directly, and to support support clinicians with less extensive experience. However, in the perspective of the new and exploded digital health field, this model is also a demonstration of the capacity health digital twin to go beyond clinical expertise. The model can contain complementary information to clinicians because of their capacity to harness more information, handle

probability distributions which are hard for humans to, and therefore give a more nuance description of, in this case, lung health. The capacity to handle more complexity can provide unique and useful insights that can be crucial for decision making in clinics.

I've explained in section X, domain expert inference evaluation is a way to verify that for simple input scenarios corresponding to well-known pathologies, the posteriors distributions matches clinicians expectations. Although this is more of a validation of model correctness, it also showcases how useful the model can be when used by patients to forge a basic understanding of their lung health in a way that is intuitive, almost gamified.

Scenario 1: Asthma

Asthma is an obstructive lung disease characterised by periodic crises that affect the airways without impacting the alveoli. Consequently, a more severe crisis corresponds to a greater drop in FEV₁. A domain expert would thus expect high airway resistance without affecting alveolar function, at least until airway resistance reaches extreme levels. In figure X, three severities of asthma crises are illustrated:

1. A moderate crisis leads to a small drop in FEV₁, reflected in the model by an airway resistance of about 30–40%, with no change in inactive alveoli.
2. A severe crisis shows a large drop in FEV₁, with airway resistance rising to around 50–60%.
3. An extreme crisis leads to a very high FEV₁ drop, and model results exceed 80% airway resistance. In this extreme state, despite compensatory mechanisms, tiny volumes of air are renewed at each breathe, and insufficient oxygen reaches the alveoli, causing oxygen saturation to fall. However, this drop is explained solely by the airway resistance and not explained by inactive alveoli that see airflow, which remains normal.

Scenario 2: Pneumonia

In pneumonia, which is essentially the opposite situation to asthma, the infection affects the alveoli. This incapacitates a large portion of alveoli and results in oxygen desaturation. Yet, it leaves airway resistance unchanged. Figure X shows two case simulations that confirm the model aligns with a clinician's expectations: alveoli become extensively damaged while the airway resistance remains normal.

Scenario 3: CF

Here, the model depicts a CF patient's progression over time. Initially, a young individual has mild lung impairment, manifesting as nearly normal airway resistance (A). After two decades, cumulative small-airway damage has caused a substantial drop increase in airway resistance even during stable periods, leading to high airway resistance (B). This chronic damage also compromises a large amount of alveoli, introducing only a small oxygen desaturation thanks to surnumerary alveoli count. Although compensatory mechanisms (e.g., blood-flow redistribution) still sustain near-normal PaO_2 , the airway resistance is now majorly reduced, putting the individual at risk of escalating symptoms. At this stage, additional blockage in the small airway due to an acute pulmonary exacerbation could marginally reduce spirometric results. The marginal change in airway resistance might be enough to overwhelm compensatory responses and trigger a noticeable oxygen saturation decline.

1.7.3 Validation against synthetically generated data

I have explained in section X that a typical way to validate a generative graphical model is to use posterior predictive checks. I have essentially replicated the Breathe dataset using the generative capabilities of the model. Given an individual with n records, I initialised the healthy variables' prior according to the individual's height, age, and sex. I initialised the lung metrics priors to the typical airway resistance and alveoli distributions in the Breathe dataset and justified this decision in the next paragraph. I then used forward sampling to obtain n synthetic datapoints from the model. By repeating this for each individuals, I could replicate the full Breathe dataset. I then produced a visual comparison of the real dataset (blue) and the synthetic dataset (green) with their respective FEV_1 -oxygen saturation plot as can be seen on figure 1.17.

I would like to make a point on the airway resistance and inactive alveoli priors I used for the forward sampling. When I was inferring the lung health metrics with uniformly distributed priors. I was assuming that the model was agnostic of the individual's lung pathology and medical history. Keeping every health state equiprobable was a way to ensure that the model would describe lung health only by capturing information from the data (model evidence). For this part of the validation, the uniformly distributed assumption is not an optimal choice. The majority of individuals have mild symptoms or became asymptomatic after starting triple therapy. I would therefore assume that an airway resistance below 50% more likely than above 50%. I needed priors that are representative of the breathe dataset. I therefore calculated the population-level health metrics by inferring the airway resistance and in active alveoli probability distributions for each record of each individual, and computing a

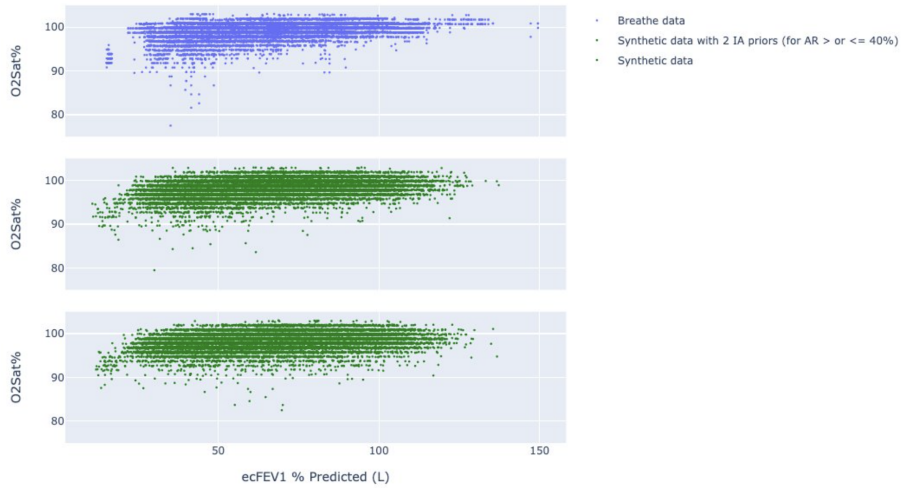


Fig. 1.17 Synthetic data vs real data comparison. – I address the middle plot later on in the section

normalised average across all records, which by the way will be shown in a future section of this validation chapter (section X).

The first and most important observation that can be made is that all the data is probable under the model. Indeed, there is a corresponding green data point in the region of every blue data point (to a small exception on the far right side of the plot that I will justify later). Concretely, this means that the true data is a subset of the synthetic data, or, in other words, that all true data-points could theoretically have been sampled from the model with a high probability. If the true data was improbable under the model, the model would be bad representation of the real world. This indicates that the model grasps all the variability in lung health present in the studied data which is already an exceptional achievement.

I can now focus on the regions that are covered by the synthetic data but not by the real data. Those regions correspond to states of lung health that are probable under the model but that have not been observed. On one hand, it indicates a degree of generalisation proving the model is not over-fitting the studied data. On the other hand, my next concern has been to understand whether the areas where with no overlap were related to plausible observations or related to observations that cannot be justified by model assumptions nor expected by a domain expert. There are two clear mismatching regions that I have to justify: i) the clear gap in the blue data on the left most side, ii) the "bottom envelope" of the data which is linear for the blue plot but rather constant for the green plot.

The clear gap on the left most side concerns is in the region of extremely high lung disease severity as shown by the predicted ecFEV₁ values between 15% and 25%. I expect that individuals reaching such low ecFEV₁ regimes would receive a lung transplant or,

unfortunately, are moved to intensive care unit. In both cases I do not expect them to record anymore data. In fact, it is rather the isolated group of blue datapoints that is surprising. Since the underlying physiological processes are continuous, although they are not linear at such low regimes as seen in figure X, I can confidently say that, if the dataset was richer, there would be observations filling this gap, perhaps with a decreasing density of records when moving left. This continuity of is present in the synthetic dataset which makes sense and is comforting to say I have chosen the realistic abstractions on the data and binning parametrisation when building the non linear factor F5 from the "top" curve in section X, despite the data scarcity in the region.

The difference in the shape of the bottom envelopes is another striking difference between the two graphs. The difference is due to the range of achievable oxygen saturation at different predicted FEV₁ regimes. For example one can see that the Breathe data is not separable because of the "linear" bottom envelope: it's unlikely to observe a high amount of inactive alveoli if the airway resistance is low, and it's unlikely to observe a low amount of inactive alveoli if the airway resistance is high. This represent the joint dependency between the IA and AR variables. I decided to not model this relationship in section X because it is specific to the manifestation of CF lung disease. Indeed in asthma it is expected to observe high AR and low IA scenarios, and in pneumonia it's expected to observe low AR and high IA scenarios. Those examples in the synthetic data are probable because the data was sampled from the AR and IA distributions separately, not jointly, and is thus separable. I could have modeled this CF-specific relationship by linking AR to IA on the factor graph as in figure X. Consequently, the prior knowledge of IA would be conditionally dependent on the inferred distribution of airway resistance. Upon building the factor F6, it would mean that the higher the AR, the smaller the tail of the IA prior would become. As a result this would limit the minimum achievable oxygen saturation values when going to the left, thus resolving the difference between the two plots.

I ran a simple experiment to verify that this modeling decision is indeed responsible for this data overlap mismatch. Instead of fully modelling the continuous tail decrease impact of AR on the IA prior, I decided to add a simple joint relationship by setting two IA priors, one for AR above 40% with a longer tail, one for AR below 40% with a shorter tail. To do so, I split the dataset in two at a threshold of 40% of airway resistance and reran the computation of the F6 factor for each dataset. I then resampled the synthetic dataset by alternating between the two IA priors given the state of AR. The second synthetic dataset's bottom profile should be closer to the one of the real data. The resulting scatter plot on figure X clearly shows that this very approximate modelling adds some linearity in the shape of the bottom envelope. I can therefore confidently confirm that the initial difference in this

envelope is caused by the decision to not model the CF specific behaviour between AR and IA.

This modelling adjustment let use even better appreciate how accurate the range of achievable oxygen saturation becomes. In absolute values, the oxygen saturation in percentage predicted have the same density distribution, with the bulk of the measurements between 100 and 92%, and then very few observations below 90% in agreement between the two plots

This is very encouraging to validate that this first milestone was an accurate and balanced representation of lung health as a whole, not over-fitting to the Breathe data, nor to the CF disease, hereby suggesting that the model could also be generalised to other chronic obstructive disorders similar to CF such as COPD and asthma.

1.8 Opportunities of model applications in healthcare

1.8.1 An digital app to let patient take ownership of their health

The model's outputs, which might initially appear like simplistic conclusions to doctors, can be quite enlightening for patients. Even if allowing individuals to experiment with different inputs on the app does not directly improve clinical symptoms, it may have a beneficial impact on their mindset. Although I did not conduct a formal clinical trial during this project, I shared the app with a few healthy volunteers and three individuals with lung disease: one with severe asthma, another with milder asthmatic symptoms, and a self-described asymptomatic CF patient. In a short amount of time, each user felt they gained insight into specific aspects of their health. They most notably liked to understand whether their lungs were larger or smaller than average. The individual with severe asthma, for example, felt especially great to understand the non-linear relationship between a drop in oxygen saturation caused by a drop in FEV₁, and how it applied in their life - I had told them that the peak expiratory flow (commonly monitored in asthma) was roughly analogous to FEV₁ for quick assessments.

Tools like this one can easily give patients a stronger sense of ownership over their health, encouraging them to be more proactive in monitoring and managing their conditions. Because effective management of chronic lung disorders often hinges on collaboration between clinicians and patients (SectionX), intuitive, personalised visualisations of lung health could significantly improve both decision-making and time-to-treatment. In conditions like CF and other chronic respiratory diseases, this has the potential to significantly enhance quality of life and life expectancy.

On a broader scale, digital tools stand to greatly advance global health. As noted in SectionX, current devices and cloud infrastructures are already capable of processing and

presenting intelligent, personalised data to individuals. The COVID-19 pandemic raised awareness about health monitoring, but many people remain unable to interpret the data due to limited medical knowledge. A user-friendly tool that bridges this understanding gap could thus make a considerable contribution to public health worldwide.

1.8.2 A digital app to democratise access to healthcare

In Section X, I have already shown how this model can deliver early warnings of lung symptoms and how easily its outputs can be interpreted to facilitate early diagnoses. I would like to further highlight the advantage of having an interpretable lung-health model that processes easily measurable physiological data via small and inexpensive electronic devices. Because the lung is a highly complex organ, general practitioners—particularly in developing countries or remote areas may not feel fully confident diagnosing respiratory conditions without specialist support typically hard to access. A user-friendly digital tool, such as this model, can increase their confidence by reinforcing fundamental lung-health concepts, enabling them to quickly verify that no details are missed, and allowing them to simulate alternative observations to assess patient risk during a consultation. Compared to searching through reference materials, an interactive and visually driven platform is far more accessible, potentially boosting adoption among doctors. In that sense, this model serves as a proof of concept for how digital tools can democratise healthcare by empowering clinicians with immediate, reliable, and interpretable guidance.

1.8.3 Population assessment and clinical-trial monitoring

Large organisations like the UK CF Trust publish annual reports on CF population-wide health indicators. Over the past several decades, CF care has vastly improved thanks to concerted efforts by healthcare professionals who consolidate clinical insights into evidence-based standards of care. Hospital staff regularly receive updated training to implement these advances, and the CF Trust’s reports are closely reviewed by clinicians and researchers. For example, these reports often document how the average FEV₁ (% predicted) changes over time. In the same spirit, the UK CF Trust could use my lung health model to track airway resistance and alveolar dysfunction, potentially offering more granular insights into the evolution of the disease burden.

As an illustration, I derived distributions of airway resistance and “inactive alveoli” for participants in the Breathe and SmartCare CF studies. I inferred the lung health metrics from their data and clinical inputs and then aggregated the posterior distributions to obtain population-level density profiles, see figure X. A shift of the distribution toward higher values

indicates greater disease severity. I can easily observe the Breathe cohort's distribution having more weight on the right than SmartCare's, implying that participants in Breathe are generally sicker, which is consistent with earlier statements (Section X). Two factors likely explain this discrepancy. i) The study selection criteria: Breathe was open to any volunteer, whereas SmartCare required a history of acute pulmonary exacerbations, thereby excluding the healthiest cases. ii) The adoption of the CFTR modulator triple therapy, which was available during Breathe but not SmartCare (section X), known to substantially improve FEV₁ for many CF individuals. Manually generating these density plots would be time-consuming and require extensive coordination among clinicians, yet for a data scientist it becomes almost effortless if the relevant data are already available.

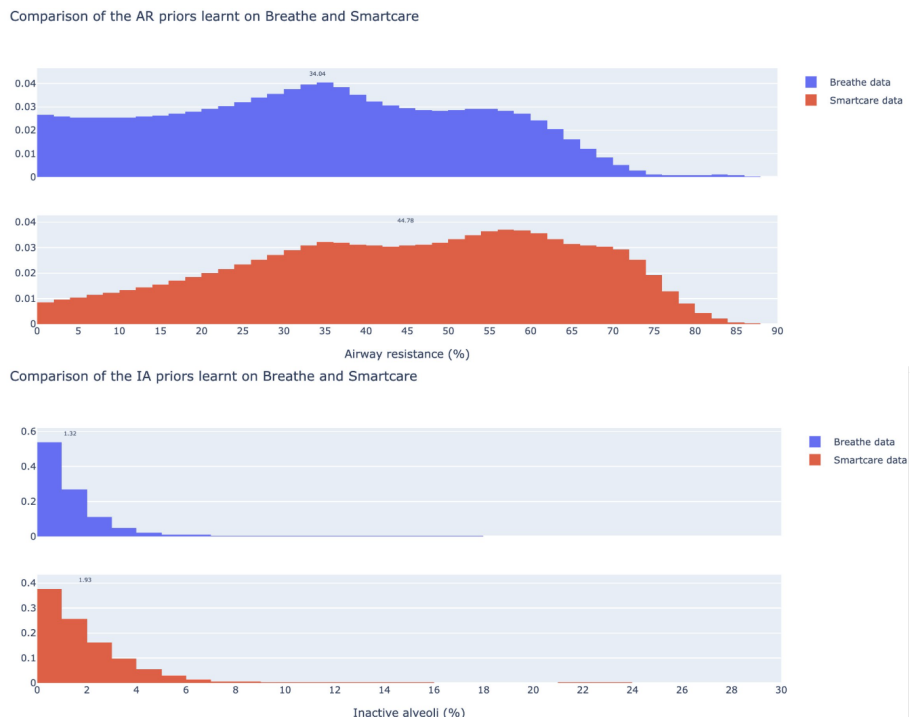


Fig. 1.18 Population-level density profile of airway resistance and inactive alveoli in Breathe vs smartcare

In a CF Trust report, population-level health demographics might rely on FEV₁ (%) predicted alone as can be seen on figure X. Although the broad conclusions remain similar, our preliminary model - despite using only two measures and limited longitudinal tracking - suggests we can achieve a clearer or more detailed signal by explicitly modeling airway resistance and alveolar function. With more data and further refinements, this approach could offer valuable new insights into the evolving health status of CF populations.

This approach also lends itself to epidemiological comparisons. For example, the European CF Trust could benchmark lung health metrics across various hospitals or countries, potentially revealing unexpected patterns and fostering impactful knowledge exchange.

1.8.4 Clinical trial monitoring

This lung health model also has a lot of potential in clinical trials applications. By comparing derived metrics, such as airway resistance and alveolar dysfunction, between a control group and a treatment group, clinical researchers gain a clearer view of how a therapy affects specific regions of the lungs. Instead of relying solely on a single measure like FEV₁ (in % predicted), this model offers detailed insights into where and how lung function changes, which can be crucial for evaluating the effectiveness of experimental treatments.

As an illustration, consider the Breathe and SmartCare CF datasets as if they represented two arms in a trial. After inferring each participant's lung health metrics (airway resistance, inactive alveoli), one can produce the posterior distributions for both groups, like on Figure 1.18 from the previous section. Cloud automations can provide the live health state of the populations during the clinical trial and also their evolution through time. By tracking how posterior distributions shift over time within each trial arm, clinical researchers can precisely identify the onset of therapeutic benefits and detect early signs of declining efficacy or emerging side effects.

1.9 Model limitations

1.9.1 Incapacity to identify small healthy lungs from big lungs with disease

The claim of a generative graphical model is that if the model is a perfect representation of the real world, than the posterior distributions will be close to point mass distribution. Hence as part of understanding the limitations of the model, I have to analyse how uncertainty is represented in the inference outputs. The most striking limitations are due to the shared uncertainty between healthy FEV and airway resistance. The model is good at identifying big healthy lungs, but it cannot differentiate small healthy lungs from big lungs with disease. I produced on figure X an example for those two cases.

The healthy FEV₁ must be equal or greater to the observed FEV because F2 is reduction factor and the opposite is not physically possible. This is a reason for the truncation of the left tail of the healthy FEV₁. At high FEV regimes (case A), associated to healthy lungs,

the truncation is so important that there is only little uncertainty remaining in the posterior distribution: the individual has bigger lungs than average.

This phenomenon does not appear in case B, leaving the uncertainty on lung size unexplained. For a given FEV_1 , the individual could either have smaller lungs than normal with a small drop due to airway resistance, or bigger lungs than normal with drop due to airway resistance, and all the situations in between. Hence, the uncertainty in lung size represented by a wide healthy FEV_1 posterior translates into shared uncertainty in lung disease severity represented by a wide airway resistance posterior.

To resolve this uncertainty, I would have to add information about lung size or to add information about disease severity that is not included in FEV and oxygen saturation. This is one of the topics that I will address in chapter X.

1.9.2 Incapacity to fully differentiate SpO_2 drop due to airway resistance or inactive alveoli

CF is characterised by the development of small airway disease resulting in a progressive increase in airway resistance that systematically comes along with aveoli damage. The two effects are joint (section X). As a result modelling general health phenomenon with CF data did not allow to fully separate the effect of one and another. Have I had excess to dataset from pathologies where this joint relationship is not present (asthma, pneumonia), I could have further calibrated the model and fully unmixed the phenomena. Since I did not have such data sets at my disposal, this is a limitation I had to accept for the rest of the project.

1.9.3 Lack of ground truth validation for inferred lung metrics

Throughout the chapter, I have always mentioned airway resistance and inactive alveoli as latent observed variables. In my exploratory work on the relationship between FEV_1 an oxygen saturation (section X), I used age as a proxy for long-term damage, and exacerbated labels as proxy from small airway damage. Since those approximations are more soft indicators, I refused to use them to evaluate the lung health metrics inferred using the model.

I have however tried to gain access to data far richer than physiological signals measured at home to validate inference results. I have specified in the model constraints that it can only read physiological signals that are easily accessible and measurable. However, more expensive measures requiring hospital equipment and train staff could be used for validation of the inferred lung health metrics. For example, a doctor could easily assess if the inferred resistance is correct for an individual by analysing CT scan. Similarly, inactive alveoli could be tested against the result of a DLCO test, or against true PaO_2 measurements.

I have tried to gain access to CT scans so that my supervisor, acting as domain expert, could evaluate the lung damage of a few individuals included in the breathe and smart care data. I would have used this lung damage scoring to cross validate my results. However, the legal specifications of the clinical trial did not allow access to CT scan scans or equivalent health records.

1.9.4 Difficulties in modelling non-linear phenomena

When I examined the factors contributing to oxygen desaturation, I recognised the significant nonlinearity introduced by the saturating nature of SpO_2 (section X). Although it turned out that the data provided enough contrast for the fitted curve, shown in Figure 1.13, to reveal the distinct physiological mechanisms at play in the lung, having access to PaO_2 data would have allowed for a more accurate representation of F5. The “top” curve would likely appear more linear, providing clearer vertical contrast and making it easier to fit the function $g(\text{AR})$ to the data.

1.10 Conclusion

In this chapter, I presented a proof-of-concept lung-health model that relies on simply two routinely accessible physiological measures, FEV_1 and oxygen saturation, yet draws heavily upon a Bayesian perspective to encode and exploit core principles of respiratory physiology. The result is a surprisingly rich representation of lung health, illustrating that even low-dimensional data can yield clinically meaningful insights when coupled with carefully structured medical knowledge and robust statistical methods.

The benefit of using a probabilistic approach: beyond clinical heuristics

A key strength of this model is that it explicitly deals with uncertainty in the variables. By probabilistically defining healthy baselines for both FEV_1 and oxygen saturation, it acknowledges that real-world data are noisy and that traditional “point estimates” (like a single predicted FEV_1) often mask important nuances. This Bayesian approach allows to easily incorporate known physiological phenomena, for instance, the saturating effect of hemoglobin dissociation, even the sex differences in normal oxygenation that rarely enter clinical practice. Each factor in the model is intentionally simple and interpretable, yet when these factors are stitched together into a coherent factor-graph, the emergent behavior captures complex, population-level trends and individual-level intricacies that go beyond clinical knowledge typically used in practice.

Clinical value and the role of digital twins

The model extends and complements the usual clinical view. Clinicians heavily rely on the FEV₁ in % predicted computed from the reference equations to assess the patient's health state. The model allows to provide a personalised estimate of the healthy FEV₁ based on the individual's data. This allows to compute FEV₁ in % healthy, which is a more accurate version of the FEV₁ in % predicted. I also implemented an analogous healthy oxygen saturation, which had not been done before. This framework paves the way for the digital twin applications, where a patient's lung function is mirrored by a computational model that can provide a synthetic view of lung health given historical physiological records, and offer interpretable predictions that can empower the clinicians to run scenario-driven tests and reason about disease progression,

Empowering patients and clinicians

The reason that grants the model its explanatory power also makes it an effective communication tool. By visualising and interacting with the model on the digital app, clinicians and patients can gain clearer insight into how a drop in FEV₁ or oxygen saturation translates into different patterns of airway resistance and alveolar dysfunction. Despite FEV₁ and oxygen saturation both being familiar to physicians, the model's ability to probabilistically combine them and compute underlying health metrics in real time is a significant step beyond typical clinic-centric heuristics. The digital app can encourage patient to take ownership of their health: they can change their habits (e.g., more frequent physiotherapy, increased activity) and evaluate the impact on lung health.

References

Appendix A

Multiplying two uniformly distributed random variables

Let us define two uniformly distributed random variables: $X \sim U(a, b)$, $Y \sim U(c, d)$, with $a, b, c, d \in \mathbb{R}_+$. Let us define a dependent random variable $Z = X \cdot (1 - Y)$. The distribution of Z is the convolution of X and Y given by:

$$f_Z(z) = \int_{-\infty}^{\infty} \frac{1}{|y|} \cdot f_X(z/y) \cdot f_Y(y) dy \quad (\text{A.1})$$

Knowing the probability density function of a random variable following a uniform distribution:

$$f_X(x) = \frac{1}{b-a} \cdot \mathbb{1}_{(a,b)}, \text{ with the indicator function } \mathbb{1} \text{ on the interval } (a, b) \quad (\text{A.2})$$

We obtain:

$$f_Z(z) = \frac{1}{(b-a)(d-c)} \int_c^d \frac{1}{|y|} \mathbb{1}_{a \leq z/y \leq b} dy \quad (\text{A.3})$$

For each increment dy , the following two inequalities must simultaneously hold:

$$\begin{cases} c \leq y \leq d, \text{ for the integral to be defined} \\ a \cdot y \leq z \leq b \cdot y, \text{ for the integral to be nonzero} \end{cases} \quad (\text{A.4a})$$

$$\begin{cases} c \leq y \leq d, \text{ for the integral to be defined} \\ a \cdot y \leq z \leq b \cdot y, \text{ for the integral to be nonzero} \end{cases} \quad (\text{A.4b})$$

With (A.4a); $a \cdot c \leq a \cdot y \leq a \cdot d$; $b \cdot c \leq b \cdot y \leq b \cdot d$, the integral is defined and nonzero when:

$$a \cdot c \leq a \cdot y \leq a \cdot d \leq z \leq b \cdot c \leq b \cdot y \leq b \cdot d \quad (\text{A.5})$$

We then resolve the integral in A.3:

$$f_Z(z) = \begin{cases} \frac{1}{(b-a)(d-c)} \int_c^{z/a} \frac{1}{|y|} dy, & \text{for } a \cdot c \leq z \leq a \cdot d \\ \frac{1}{(b-a)(d-c)} \int_c^d \frac{1}{|y|} dy, & \text{for } a \cdot d < z < c \cdot b \\ \frac{1}{(b-a)(d-c)} \int_{z/b}^d \frac{1}{|y|} dy, & \text{for } c \cdot b \leq z \leq b \cdot d \end{cases}, \text{ when } a \cdot d \leq c \cdot b \quad (\text{A.6})$$

This result in **the closed form solution for the multiplication of two uniformly distributed random variables.**

$$f_Z(z) = \begin{cases} \log\left(\frac{z}{a \cdot c}\right), & \text{for } a \cdot c \leq z \leq a \cdot d \\ \log\left(\frac{d}{c}\right), & \text{for } a \cdot d < z < c \cdot b \\ \log\left(\frac{d \cdot b}{z}\right), & \text{for } c \cdot b \leq z \leq b \cdot d \end{cases}, \text{ when } a \cdot d \leq c \cdot b \quad (\text{A.7})$$

Note: When $a \cdot d > c \cdot b$, the second term of the closed form solution gest more complex because of overlapping intervals. The solution can be found by swapping the variables X and Y to come back to the case where with $a \cdot d \leq c \cdot b$.